AGU PUBLICATIONS

JGR

Journal of Geophysical Research: Space Physics

RESEARCH ARTICLE
10.1002/2016JA022481

Key Points:
- Energy-banded ions from tens to ten thousands of eV are observed
- They are observed in every large storm encountered by the FAST satellite
- Contrary to existing theory of band generation, different species are observed at the same energies

Correspondence to:
C. A. Colpitts,
chrisc@fields.space.umn.edu

Citation:
Colpitts, C. A., C. A. Cattell, J. U. Kozyra, M. F. Thomsen, and B. Lavraud (2016), Satellite observations of energy-banded ions during large geomagnetic storms: Event studies, statistics, and comparisons to source models, *J. Geophys. Res. Space Physics*, *121*, 6353–6377, doi:10.1002/2016JA022481.

Received 3 FEB 2016
Accepted 14 JUN 2016
Accepted article online 16 JUN 2016
Published online 14 JUL 2016

Satellite observations of energy-banded ions during large geomagnetic storms: Event studies, statistics, and comparisons to source models

C. A. Colpitts[1], C. A. Cattell[1], J. U. Kozyra[2], M. F. Thomsen[3], and B. Lavraud[4]

[1]School of Physics and Astronomy, University of Minnesota, Minneapolis, Minnesota, USA, [2]Department of Physics, University of Michigan, Ann Arbor, Michigan, USA, [3]Los Alamos National Laboratory, Los Alamos, New Mexico, USA, [4]Institut de Recherche en Astrophysique et Planétologie, Toulouse, France

Abstract Energy-banded ions from tens to ten thousands of eV are observed in the low-latitude auroral and subauroral zones during every large (minimum $Dst < -150$ nT) geomagnetic storm encountered by the FAST satellite. The banded ions persist for many FAST orbits, lasting up to 12 h, in both the northern and southern hemispheres. The energy-banded ions often have more than six distinct bands, and the O^+, He^+, and H^+ bands are often observed at the same energies. The bands are extensive in latitude (~50–75° on the dayside, often extending to 45°) and magnetic local time, covering all magnetic local time over the data set of storms. The distributions are peaked in the perpendicular direction at the altitudes of the FAST satellite (~350–4175 km), although in some cases the precipitating component dominates for the lowest energy bands. At the same time, for some of the events studied in detail, long-lasting intervals of field-aligned energy dispersed ions from ~100 eV to 40 keV are seen in Los Alamos National Laboratory geosynchronous observations, primarily on the dayside and after magnetosheath encounters (i.e., highly compressed magnetosphere). We present both case and statistical studies of the banded ions. These bands are a new phenomenon associated with all large storms, which are distinctly different from other banded populations, and are not readily interpreted using previous models for particle sources, transport, and loss. The energy-banded ions are an energetically important component of the inner magnetosphere during the most intense magnetic storms.

1. Introduction

Major geomagnetic storms trigger a wide range of changes in the Earth's magnetosphere, inluding the transfer of a significant amount of energy, and are usually associated with coronal mass ejections, large interplanetary magnetic fields, and/or high-pressure solar wind plasma [*Baker et al.*, 2001]. There are many unusual particle acceleration processes that can occur, including prompt energization of relativistic electrons in the radiation belts [*Wygant et al.*, 1994], acceleration of electrons over a broad energy range in the auroral zone [*Shiokawa et al.*, 1996; *Dombeck et al.*, 2005; *Nakajima et al.*, 2007], and strong outflow of ionospheric ions in the polar cap [*Moore et al.*, 1999; *Strangeway et al.*, 2000]. Although much of the research on storms in the auroral zone has focused on electrons, including those that produce subauroral red (SAR) arcs and great red aurora [*Kozyra et al.*, 1993, 1997; *Shiokawa et al.*, 1997], there are unusual signatures in the ions that are seen during large storms and which are sometimes coincident with these electron signatures.

During superstorms (defined as $Dst < -240$ nT by *Mac-Mahon and Gonzalez* [1997]), the surprising discovery was made that soft (<1 keV) ions penetrate deep within the plasmasphere—as low as 33° magnetic latitude (MLAT) ($L \sim 1.4$) [*Swider*, 1990; *Huang et al.*, 2005]. This is much deeper than is possible for ions to drift inward from the magnetotail and remain within this energy range; thus, the source of these ions is unknown. FAST observations revealed that these ions often had multiple energy bands [*Thomsen et al.*, 2004; *Cattell et al.*, 2004; *Kozyra et al.*, 2004] ranging from 10 eV to 10 keV. As shown in *Colpitts et al.* [2012] and demonstrated later in this paper, multiple ion species appear in a single energy band; thus, this banding cannot be explained by currently known mechanisms which organize bands by constant velocity rather than constant energy seperating ion species into different bands. Defense Meteorological Satellite Program (DMSP) observations indicated that the soft ions appeared first without banding and then later developed this feature. However, these observations were made at ~850 km altitude by satellites in the Defense Meteorological Satellite Program (DMSP) and thus viewed only the precipitating component. In contrast FAST observations revealed a higher-energy component with a double loss cone distribution

not seen at DMSP altitudes. The source of these ions and their evolution to multiple energy bands are major focus areas of ongoing research.

The banded ions are often accompanied by plasma waves banded in frequency [*Parrot et al*., 2006; *Colpitts et al*., 2012]. These banded ions are part of a phenomenology of subauroral to midlatitude features, which includes unstructured and structured warm (tens to ten thousands of eV) ion distributions (both multiple energy bands and wedge-like ions) with possibly multiple source mechanisms that span three regions during superstorms: (1) the diffuse auroral region, (2) the region between the diffuse aurora and the plasmasphere, and (3) plasmaspheric field lines. Taken together, these features provide clues to the mechanisms that transport warm ions into the inner magnetosphere during superstorms. At these times, warm ions can provide up to 30% of the intense ring current energy in the dawn sector [cf. *Hamilton et al*., 1988] making them an energetically important component during extreme events. The deeply penetrating warm ions (particularly the protons) transfer considerable energy to the thermal electrons through Coulomb collisions supplying an additional energy source for the subauroral electron temperature peak and SAR arcs and altering the energetics of the subauroral region. A better understanding of the details of this phenomenology and how its elements are interrelated is needed to place constraints on source mechanisms and trace associated effects throughout the geospace system.

In this paper, we focus on warm ($<$10 keV) ions with multiple energy bands in order to better understand the morphology and evolution of this population. These ions, banded in energy from 10 eV to 10 keV, were first reported in conjunction with studies of the October 2003 "Halloween" magnetic storms [*Thomsen et al*., 2004; *Cattell et al*., 2004; *Kozyra et al*., 2004]. The energy-banded ions during the Halloween storms lasted for more than 12 h, often had more than six distinct bands, and the O^+ and H^+ bands were sometimes at the same energies. The bands were evident on both dayside and nightside and were extensive in latitude (~50–75° on the dayside, often extending to 45°, the low-latitude limit of the FAST observations). The distributions peaked in the perpendicular direction (locally mirroring) at FAST altitudes.

Energy-banded ions have previously been reported on auroral field lines at low altitudes (FAST, DMSP, and DE-2), intermediate altitudes (DE-1), and at high altitudes (Polar and Cluster). In the low-altitude auroral zone, energy-dispersed discrete bands, which lasted for a few hours and had equal O^+ and H^+ velocities, have been reported during quiet times. Two interpretations for the observed structures were proposed [see, e.g., *Boehm et al*., 1999, Plate 1]: (1) convective drift dispersion from an ionospheric heating source [*Hirahara et al*., 1997] and (2) time-of-flight dispersion from an equatorial acceleration event [*Boehm et al*., 1999]. Both models predict that O^+ and H^+ ions will have the same velocity, that energy bands have ratios dependent on latitude (field line length), and that energy increases with latitude. The equatorial source model assumes an impulsive acceleration process that is broad in latitude, as described by *Mauk* [1986]. Examples include substorm injections and compression of the magnetosphere by high solar wind dynamic pressure. The observed energy dispersion with latitude depends on the length of the field line square and results in bands in energy with ratios of $[0.25, .75, 1.25\ldots]^2$. In the ionospheric acceleration model, the latitude dispersion depends on the $E \times B$ drift velocity and results in bands with ratios of $[1, 2, 3\ldots]^2$ or $[1.5, 2.5, 3.5\ldots]^2$. *Boehm et al*. [1999] concluded that both their observations and those of *Hirahara et al*. [1997] were most consistent with the equatorial acceleration mechanism.

A statistical study of O^+ and H^+ ions using FAST data over the year 2000 also identified features with multiple-energy bands [*Yao et al*., 2008]. They concluded that the hydrogen and oxygen bands had different source mechanisms because they had different occurrence probabilities and locations. The H^+ bands generally were observed at higher latitudes within the auroral oval and during quiet times, whereas the O^+ bands occurred at lower latitudes around the equatorward boundary of the auroral oval during more active intervals. They concluded that the oxygen bands were consistent with a velocity filter from higher to lower latitudes and that the bands may supply oxygen from the ionosphere to the ring current during storms. Since keV protons in an ionospheric plasma (1000–2000 cm^{-3} with electron temperature of 0.5 eV) have a Coulomb loss lifetime of 1–2 h compared to 0.5–1 day for oxygen [cf. *Kozyra et al*., 1987], these bands may initially have been a mixture of the two species with the protons being rapidly depleted by Coulomb collisions leaving the bands dominated by oxygen.

Using DE data (at low altitudeand midaltitude), *Frahm et al*. [1986] and *Winningham et al*. [1984] described energy-dispersed ion bands, within the region of diffuse aurora, from a few eV to a few keV and peaked at

a pitch angle of 0°. In contrast to the *Boehm et al*. [1999] and *Hirahara et al*. [1997] observations, these occurred primarily during the main phase of storms. Similar to *Hirahara et al*. [1997], the bands were interpreted as being the result of convective dispersion from an ionospheric, auroral source.

At higher altitudes, Polar observations of multiple energy-dispersed bands (approximately ones to hundreds of keV) were reported by *Fennell et al*. [1998] and *Peterson et al*. [1998]. These events had O^+ and H^+ at the same energy and were weakly peaked at 90°-pitch angle. They extended from L ~ 3–8, were most often seen from ~06:00 to 18:00 magnetic local time (MLT), and in quiet times following substorms. Three different explanations were proposed: (1) convection of time variable discrete ion sources in the plasma sheet [*Peterson et al*., 1998], (2) time-of-flight following prompt energization in an electric field pulse associated with substorm dipolarization with bands dependent on grad B drift time [*Li et al*., 2000], and (3) time-varying $E \times B$ convection of a tail source population for energies $>$ ~1 keV and an ionospheric source for energies $<$ ~1 keV [*Fennell et al*., 1998]. A subsequent particle tracing simulation [*Ebihara et al*., 2004] concluded that the *Fennell et al*. mechanism was most likely, with the bands being a result of enhanced convection (during the substorm) followed by reduced convection.

Note that there are other band-like features that have been observed and modeled, including the ion "gaps" [see, e.g., *Kovrazhkin et al*., 1999], "wedge"-type dispersion [*Ebihara et al*., 2001], and velocity-dispersed ions in the plasma sheet boundary layer [*Ashour-Abdalla et al*., 1992, 2005; *Bosqued et al*., 1993]. During superstorms, ion distributions resembling wedge-like ions frequently appear as an important component at the lowest latitudes overlapping with the banded ions. These low-latitude warm ion structures have also been described as injections into the low-energy tail of the ring current distribution by *McFadden et al*. [2001]. These are essentially complementary descriptions of the same phenomena, which is not treated in the present study. Many of these previously reported band-like structures are observed during some of the events with ion banding shown herein and can be co-located with the bands, but are different phenomena; warm energy-banded ions at constant energy across all component species such as these have not previously been reported.

Wave emissions with harmonics near the ion cyclotron frequency are also seen during large geomagnetic storms. The occurrence of harmonic emissions in the DEMETER wave data in association with large storms was first described by *Parrot et al*. [2006]. The fact that energy banded ions were also seen during these intense storms led *Colpitts et al*. [2012] to investigate the association of the two phenomena, utilizing both particle data and wave data from the FAST satellite. Details of the relationships between the short-lived (in the satellite frame) waves seen on DEMETER and both the banded ions and a different type of banded VLF emissions are discussed in *Colpitts et al*. [2012]. The banded waves and ions were observed in all 26 large (minimum $Dst < -100$ nT) storms investigated, and it was determined that the waves could be generated by the banded ions, although the exact free energy source was not definitively identified.

There is some evidence to suggest that banded ions are also observed on the same field lines as the banded waves reported by *Parrot et al*. [2006] in the trough region. See, for example, the discussion of the trough region banded waves in *Colpitts et al*. [2012] during the 7–10 November 2004 superstorms at L = 2.3–3.0 in the DEMETER data on the nightside in their Figure 2 and the observations of banded ions on these same L values at this same time but on the dayside in the FAST data in their Figure 1. The same is true on 21 January 2005 for DEMETER at 20:09 UT (9.7 MLT) and FAST at 20:07 UT (1.7 MLT) in the northern hemisphere. Since the phenomenon of banded ions covers virtually all MLTs and the heating of the thermal plasma by the banded ions contributes to the subauroral T_e peak, which is also extended over all MLTs, the observations by DEMETER and FAST on the same L values but different MLTs offer valid support for the relationship between banded ions and trough region banded waves, suggesting that they are part of the overall phenomenology during superstorms.

In this paper, we address the occurrence of these energy-banded ions during large storms [*Bell et al*., 1997; *Mac-Mahon and Gonzalez*, 1997]. As we will show, these ions are a distinctly different population from previously reported ion bands and are associated with unique characteristics of strong geomagnetic storms. Potential source populations, energization, and loss mechanisms will be discussed. The role of this ion population in superstorm dynamics will be briefly addressed. The paper will present case studies of three superstorms and one strong storm that provide a range of driver conditions that can be used to illuminate the origin and effects of these ions, as well as statistical data on the ion band occurrence. The data sets utilized are described in section 2. The revealing example of energy banded ions from the 29–31 October 2003

Halloween superstorm is discussed in section 3. The three other exemplary events—07–11 November 2004, 20–24 November 2003, and 26–31 August 1998—are presented in section 4. Statistical results on the occurrence of banded ions during the set of 11 superstorms and 26 large storms are presented in section 5, and a detailed comparison of the geosynchronous observations with previous models is given in section 6. Discussion and conclusions are given in section 7.

2. Instrumentation and Data Sets

The data presented in this study comes primarily from the FAST satellite, with additional data from Los Alamos National Laboratory (LANL) instruments on geosynchronous satellites provided for the case studies. The complete features of the FAST particle instrumentation are presented in *Carlson et al.* [2001] for the electrostatic analyzers and *Klumpar et al.* [2001] for the ion mass spectrometer, TEAMS (Time-of-flight Energy Angle Mass Spectrograph), and most of the data presented herein are from these two instruments. The field instruments are described by *Ergun et al.* [2001] (the electric field and waves instrument) and by *Elphic et al.* [2001] for the DC and search coil magnetic field instruments. In the initial years of the mission, instruments were turned on and data were usually limited to auroral latitudes (>60° invariant latitude (ILAT)). After 1999, data were regularly obtained at lower latitudes. For three of the four illustrative events shown here, data were obtained down to 45° invariant latitude.

A series of 13 geosynchronous satellites carrying the LANL particle instruments were launched from 1976 to 2002 into geosynchronous (6.6 R_E, equatorial) orbit with ~10 s spin rates. The last five of these satellites carried Magnetospheric Plasma Analyzers (MPA) covering electrons and protons ~1 eV–40 keV [*Bame et al.*, 1993], data from which are shown here.

In addition, data from the ACE satellite are used to provide information on solar wind conditions. Both magnetic field [*Smith et al.*, 1999] and plasma data [*McComas et al.*, 1999] are used. *Dst* data were obtained from the World Data Center for Geomagnetism, Kyoto *Dst* index service.

3. The Prototype Case of the Halloween 2003 Storms

The Halloween storms of 24 October to 5 November 2003 have been studied extensively (see, e.g., the AGU Special Collection "Violent Sun-Earth Connection Events of October–November 2003, Introduction [*Gopalswamy et al.*, 2005]) and are among the most severe events of the satellite age. The two storms on 29–30 October and 30–31 October, in particular, featured Earth-directed CMEs with speeds up to 2200 km/s, allowing for a Sun-Earth transit time of just ~19 h, and the geomagnetic response was fast and intense, with maximum running *Ap* indices of 252 and 221 for the two storms, both among the 16 largest values ever recorded. Unfortunately, these storms were so intense that ACE and Wind solar wind plasma measurements were unavailable due to contamination from the high fluxes of energetic particles, but *Skoug et al.* [2004] used 1-D Maxwellian fits to the low-resolution data to estimate the solar wind speed, density, and temperature, with estimates of 2240 km/s (29 October) and 1710 km/s (30 October) for the maximum flow speeds associated with these two storms.

Figure 1 shows the ACE magnetic field measurements, FAST ion data, and the *Dst* level (from the Kyoto World Data Center for Geomagnetism) for the 5 day period from 28 October to 01 November. The two shock fronts are evidenced by the sharp rise in the interplanetary magnetic field (B_{mag}; Figure 1a) at ~06:00 UT on 29 October and 16:20 UT on 30 October, which are followed by periods of strong southward B_z (Figure 1d). After the first shock, there is an ~12 h delay before the interplanetary magnetic field (IMF) turns southward; it reaches 25 nT and remains southward for ~9 h, while after the second shock, there is an ~3 h delay; it reaches 30 nT and does not turn northward for ~4 h. The *Kp* index (not shown) reaches 9° at about ~20:00 UT, indicating the highest level of geomagnetic activity. The *Dst* (Figure 1f) shows two very large drops corresponding to the two storms. Figure 1eshows the FAST ion spectrograms, to indicate when in the storm we have FAST ion observations, illustrating the orbital period and several data gaps where there is no ion data for a number of orbits due to data rate and antenna availability. The *y* axis is energy in log form from 4 to 30,000 eV, and the color scale is log of energy flux. At this time resolution there is no way to resolve the energy-banded ions (or any other feature—the data are merely presented here to show when FAST ion data are available), but the orbits in which we observe ion bands are indicated by the magenta bands at the top of

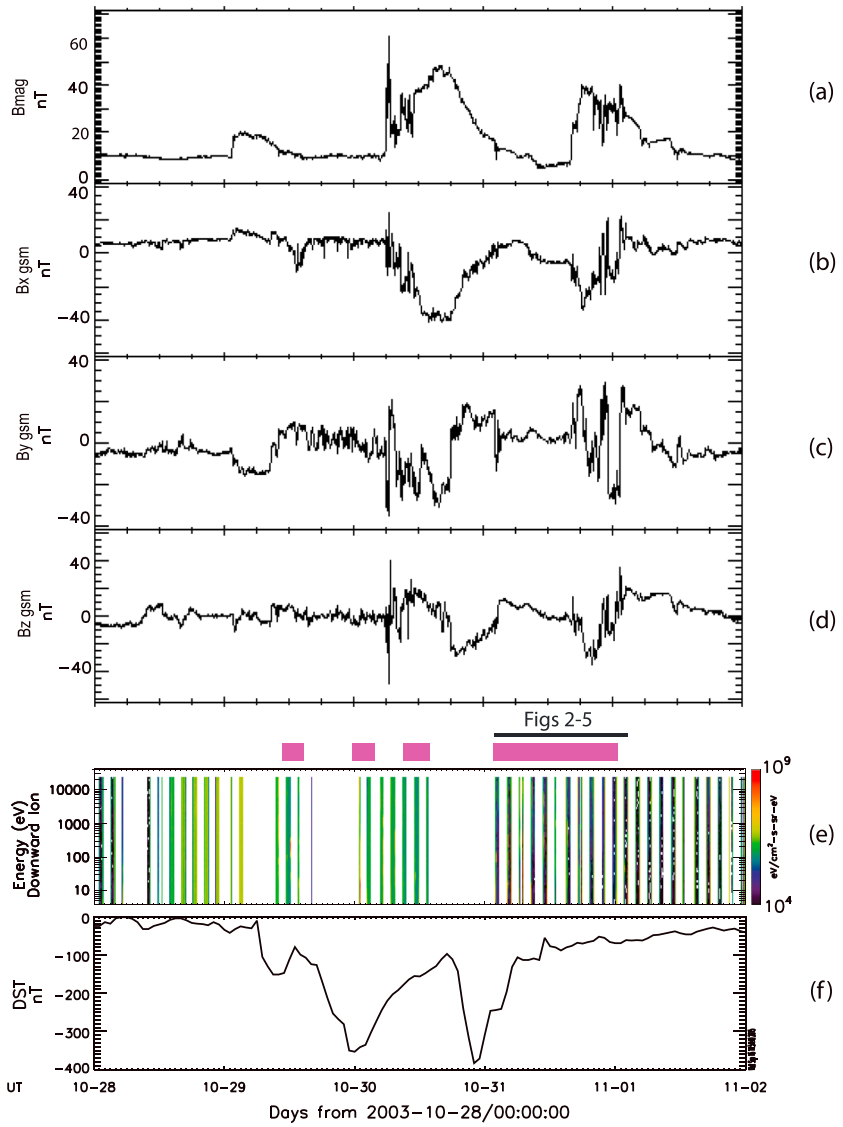

Figure 1. ACE magnetic field measurements of (a) magnitude of B (B_{mag}), (b) GSM B_x, (c) GSM B_y, and (d) GSM B_z (north-south component of B). (e) FAST ion spectrograms showing all times when FAST ion data were taken during the storm (the magenta bars above this panel represent orbits in which banded ions are observed; the black bar and "Figures 2–5" indicate the orbits which will be shown expanded in subsequent figures). (f) *Dst* level (from the Kyoto World Data Center for Geomagnetism) for the 5 day period from 28 October to 01 November 2003.

the panel. The orbits that will be expanded and plotted in subsequent figures are indicated by a black bar above the magenta bar and the label "Figures 2–5." The magenta bands (in this figure as well as Figures 8, 11, and 13) include both dayside and nightside observations of banded ions (both for most orbits), as there is no correlation between phase of storm and observation of bands in the dayside, nightside, or both.

Figure 2 shows six consecutive dayside (MLT of ~08:00 to 11:00) auroral passes on 31 October 2003 covering the time period 01:54–13:06 UT, but plotted versus latitude rather than UT. From left to right, the panels are energy spectrograms of ions with perpendicular (60–120°), upgoing (150–180°), and downgoing (0–30°) pitch angles (these ranges are used for all subsequent pitch angle sorting as well) for the six orbits, with energy in log form from 4 to 30,000 eV on the y axis, latitude from 45 to 85° south on the x axis, and the log of the energy flux in color scale. Several ion bands are visible in the downgoing and perpendicular components, at energies from tens of eV to tens of keV, lasting the entire >11 h, over a wide range of latitudes from ~50 to 75° (more commonly 56–72°).

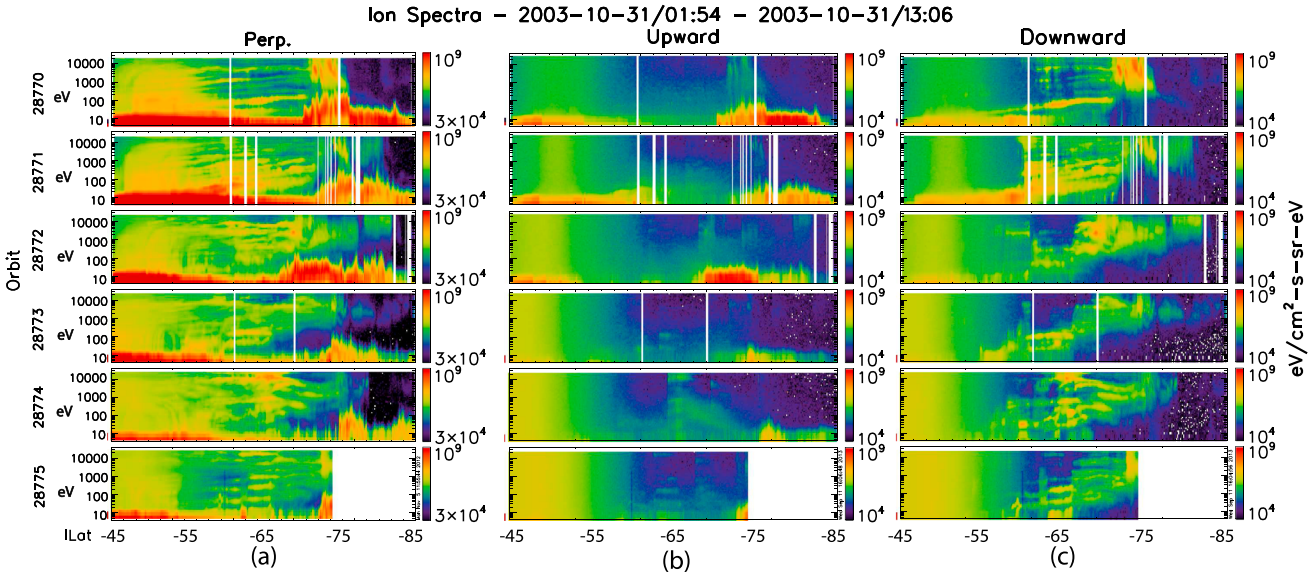

Figure 2. FAST energy spectrograms of ions with (a) perpendicular (60–120°), (b) upgoing (150–180°), and (c) downgoing (0–30°) pitch angles for six consecutive dayside (MLT of ~08:00 to 11:00) auroral passes on 31 October 2003 covering the time period 01:54–13:06 UT, with energy in log form from 4 to 30,000 eV on the *y* axis, latitude from 45 to 85° south on the *x* axis, and the log of the energy flux in color scale.

Below these latitudes and extending to 45° is the subauroral region associated in the magnetosphere with the ring current peak flux and in the ionosphere with the subauroral electron temperature peak and SAR arcs. This region is very important to subauroral energetics during superstorms. At this time DMSP F13 observed the subauroral electron temperature peak spanning the interval ~44–51° latitude at dawn and dusk, reaching

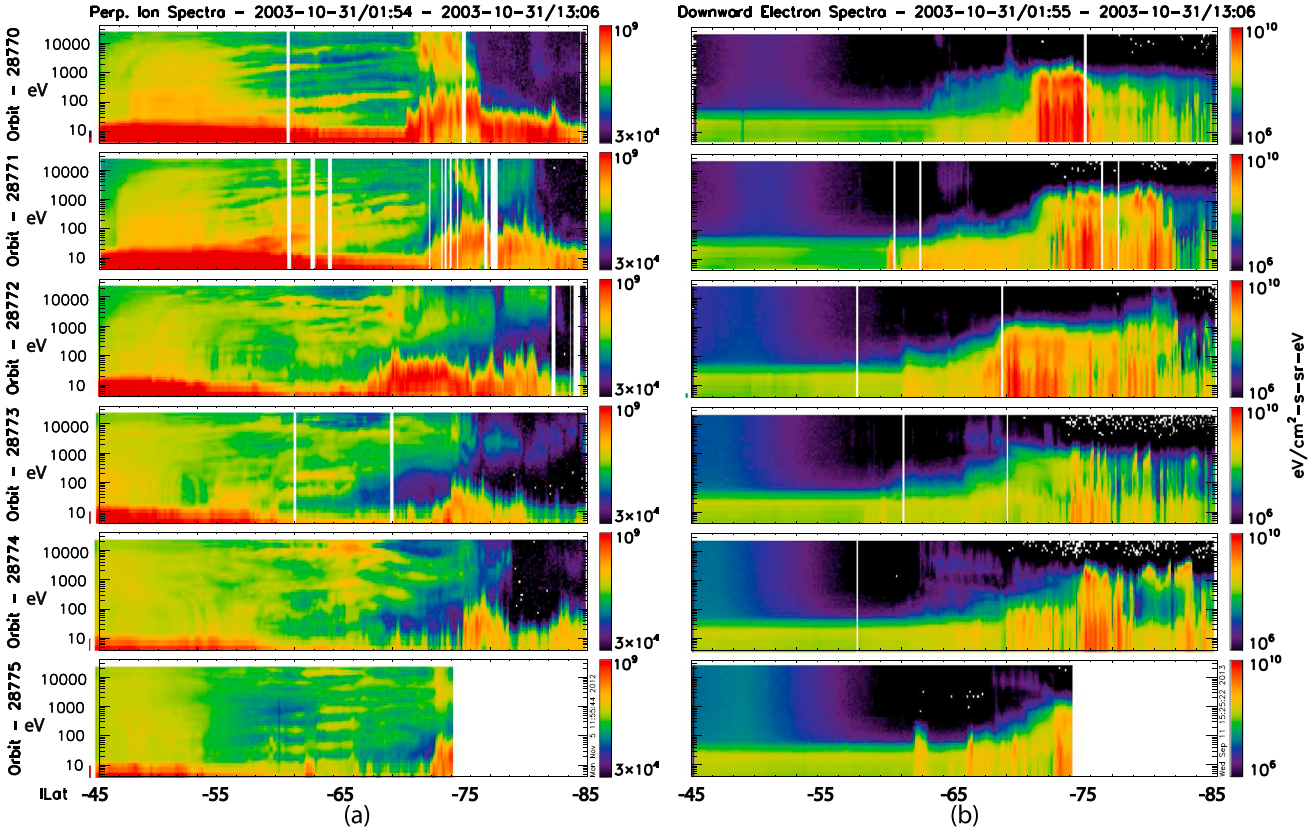

Figure 3. (a) Perpendicular ions and (b) downgoing electrons for the same passes and in the same format as Figure 2.

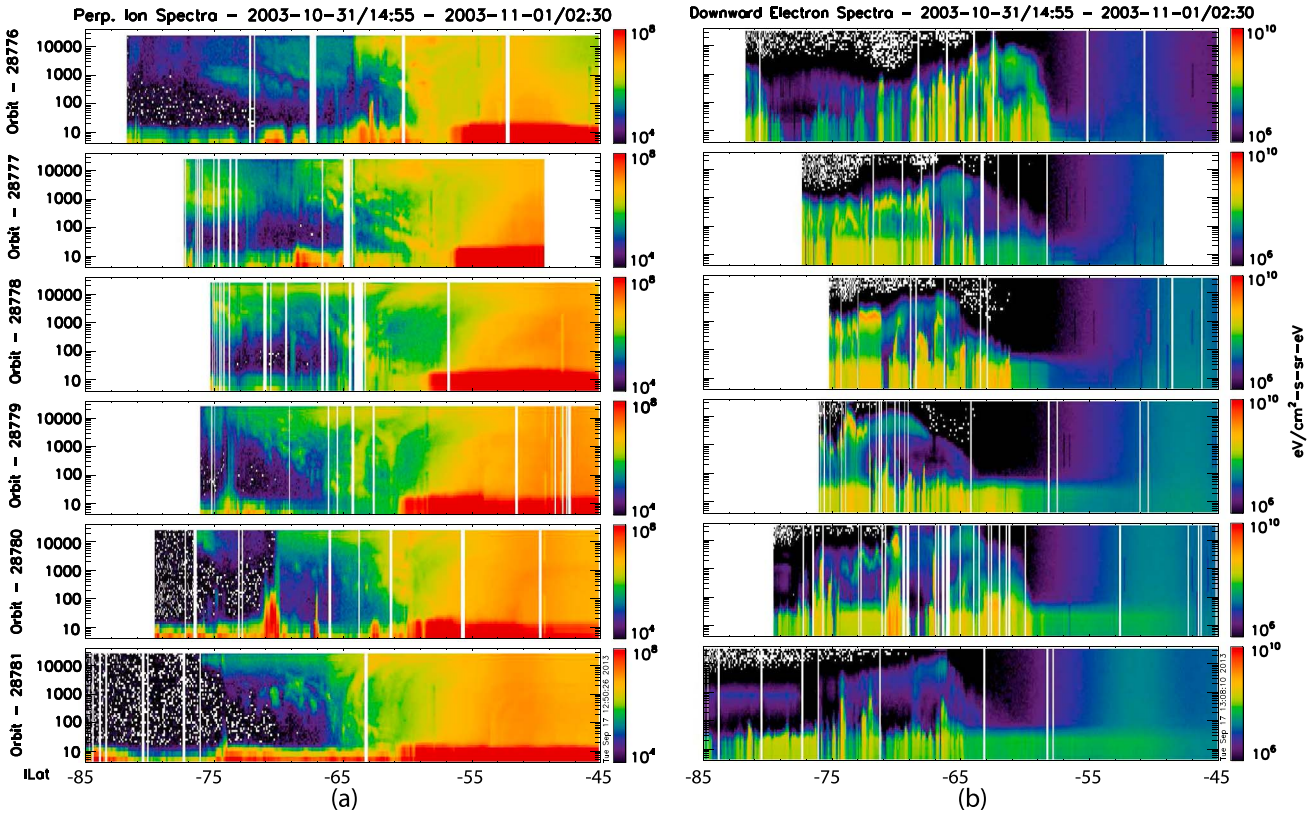

Figure 4. Energy spectrograms of (a) the perpendicular component of ions and (b) the downgoing component of electrons observed on the nightside (MLT ~ 15:00–22:00) during the six orbits immediately after the six orbits of dayside ions shown in Figure 2.

8000 K at the beginning of the interval and dropping below 6000 K by the end. The subauroral temperature peak is produced by the transfer of energy between ring current ions and thermal plasmaspheric electrons and thus identifies the region of overlap between the ring current and plasmasphere. The bulk of the energy transfer actually occurs equatorward of the clear ion energy bands, where the overlap between these ion energy bands and wedge-like ion distributions is partially obscured on the FAST spectrograms by penetrating radiation from the high-energy ring current and radiation belts. In other storms in which the penetrating radiation is weaker, wedge-like ion distributions are sometimes observed overlapping with the most equatorward segment of the banded ions.

During some orbits, there is evidence for local modification of the band energy, possibly due to local potential drops, e.g., the gradual drop and subsequent rise of the energy in the bands at latitude ~67–76° visible in orbit 28774. The banded ions are observed primarily equatorward of and within the main auroral zone, although in some passes, they extend to latitudes where the injected cusp ions are observed (e.g., top three passes near ~70–75°). The ion fluxes peak near 90°, with almost no upgoing ions, consistent with mirroring close to the satellite altitude and loss to the atmosphere of ions in the loss cone (the few observed upgoing ions in the latter three orbits likely mirror below FAST, while the majority of the mirroring occurs above the satellite). The lower energy bands, in particular, are evident in the downgoing component, while the higher energy bands are in some cases restricted to the perpendicular population (e.g., bands at latitudes 56–67° in orbit 28773). Downgoing lower energy ions consistent with the FAST observations of the precipitating lowest energy bands are seen over the same range of magnetic latitudes by DMSP satellites during this storm [*Huang et al.*, 2007], although the peaks of their observations occur during the gaps in the FAST ion data visible in Figure 1. The persistent banding was not clear in the DMSP observations.

As mentioned above, cusp ions are also evident at low (~10–200 eV) energies and high (67–85 ILAT) latitudes in this figure, and the cusp often appears to represent the poleward boundary of the banded ions. This is a common feature in the banded ion observations, although the cutoff is in many cases not very sharp

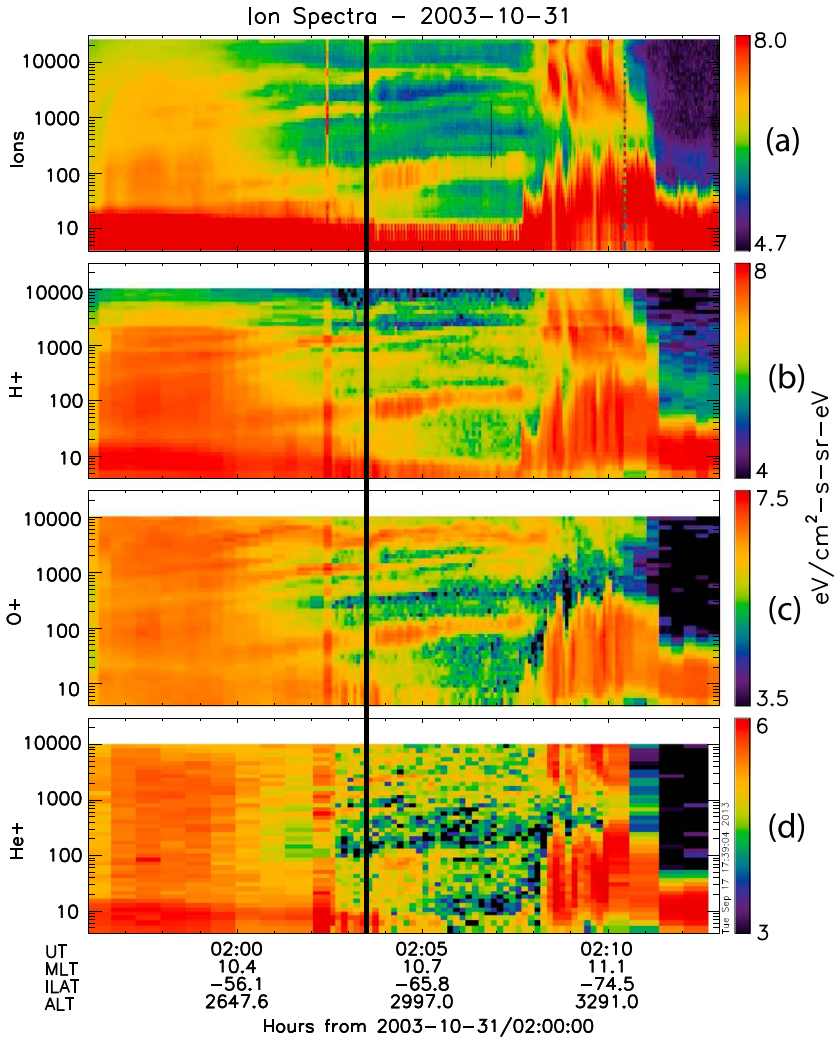

Figure 5. Energy spectrograms of (a) all ions, (b) H^+, (c) O^+, and (d) He^+ for the first orbit shown in Figure 2, from 01:56 to 02:13 UT (~50:00–80:00 ILAT). The bands are evident in all of the component species, and often at the same energy in different species (e.g., the ~100 eV and ~1000 eV bands evident in both H^+ and O^+ and to a lesser extent, He^+ from ~02:00 to 02:09) and therefore cannot be time of flight, velocity dispersion from a common source. The black vertical line indicates time of data shown in Figure 10.

(e.g., orbit 28772, where both bands and low-energy ions are evident at ~67–70 deg ILAT). The question of whether the banded ions are present on open field lines in the cusp is therefore an open one, but they are far more common on the closed field lines in the auroral zone, and if they are present in the equatorward edge of the cusp they quickly disappear at higher latitudes. Further investigation of the poleward boundary of the banded ions and their presence (or lack thereof) on open field lines could provide information as to their generation mechanism and will be a part of the more rigorous planned statistical study discussed in section 7.

Examples of the different relationships that are observed between downgoing electrons and the banded ions are shown in Figure 3, which plots the perpendicular ions (Figure 3a) and downgoing electrons (Figure 3b) for the same passes as Figure 2. Inverted-V electron signatures are evident in the top five panels, e.g., in the second panel at ~75–76, 79, and 80°. In all panels (particularly the first panel at ~73–67°, the second panel at ~76–77, and the third panel at ~70–74°), broadband electrons up to ~1 keV can be seen. In addition to the ion banding, which is equatorward of these electron features, there was strong perpendicular ion heating and ion outflow at energies $<$ ~100 eV at the same latitudes as the observed electrons, in the cusp and auroral zone in association with both "inverted-V" and broadband electron acceleration. Note that FAST

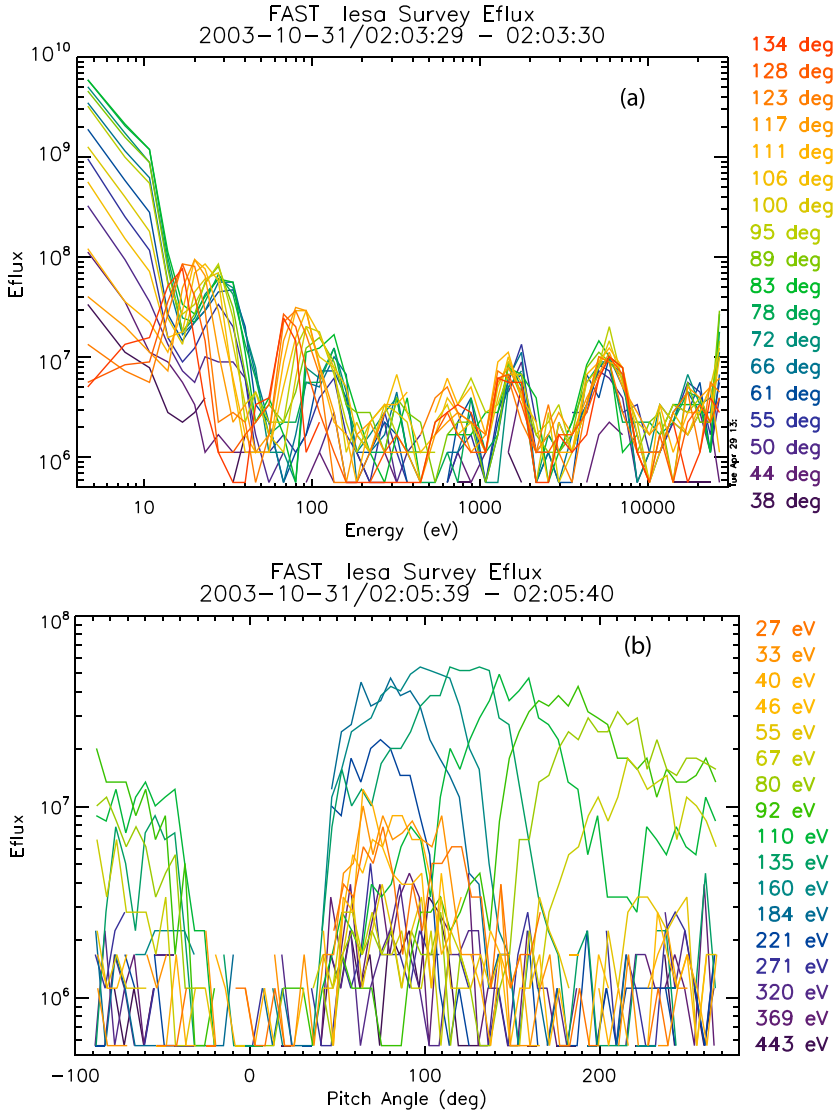

Figure 6. Ion distribution for the 1 s snapshot at 02:03:29–02:03:30 in two different formats: (a) energy flux as a function of energy with pitch angle in color scale and (b) energy flux as a function of pitch angle with energy in color scale. The bands at ~20 eV and ~100 eV visible as peaks in Figure 6a have clear pitch angle dispersion, with the lower energy components (left section of the peak) having higher pitch angles (~123–134°, red and orange) and the higher energy components closer to perpendicular (~72–95°, blue and green).

observed very intense ion outflow (of both H^+ and O^+), peaking at $>10^{10}$ ions/cm^2 s throughout this interval, consistent with previous observations of ionospheric outflow during large geomagnetic storms [*Moore et al.*, 1999]. The outflow may provide a source population for bands observed at later times.

The banding seen on the nightside is often more complex and intermittent than on the dayside, as can be seen in Figure 4, which shows energy spectrograms of the perpendicular component of ions (Figure 4a) and the downgoing component of electrons (Figure 4b) observed on the nightside during six orbits within the same storm. The orbits shown are those immediately after the six orbits of dayside ions shown in Figure 2, as the nightside bands are less evident during the timespan shown in that figure. During this particular storm, the nightside bands were more prevalent during the recovery phase, though as previously mentioned there is no consistent correlation between storm phase and dayside/nightside observations. As with the dayside ions, ion bands across the energy range from tens of eV to tens of keV are visible and persistent through the six orbits (~10.5 h); but in this case the bands exhibit energy dispersion, with higher energies observed at higher latitudes, and the ion bands only rarely occur at latitudes above ~65°.

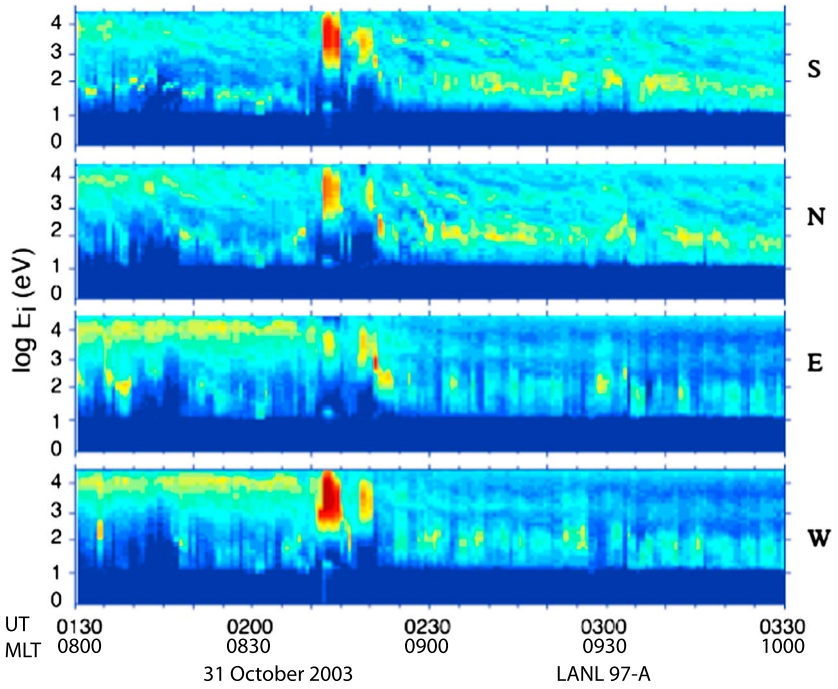

Figure 7. Energy spectrograms from the LANL-97A geosynchronous satellite during the time of the last orbits in Figures 2 and 3, when LANL-97A was on the dayside and in relatively close conjunction with FAST. The banded ions are evident in all look directions, but most prominently in the field-aligned directions (north and south), with clear energy dispersion.

However, as on the dayside, the bands are equatorward of the primary auroral electron acceleration, evident in Figure 4bas large-scale inverted-V electron signatures, e.g., in the third panel at ~74 and 72–21°, and occasionally as broadband electron acceleration (~74°; Figure 4, fourth panel), both of which are again associated with ion outflow in the auroral zone and the cusp region (not shown). Intense ion outflow was less common on the nightside but was observed during orbit 28780. Of course, ion outflow peaks near the polar cap boundary, and the electron spectrograms in Figure 4bindicate that data were not taken in this region for several of these orbits (orbits 28797–28799, data gaps above ~75°.)

Figure 5 shows the energy spectrograms of all ions, H^+, O^+, and He^+ for the first orbit shown in Figure 2, from 01:56 to 02:13 UT (~50:00–80:00 ILAT). The bands are evident in all of the component species, and although the relative flux varies from peak to peak, the bands are often observed at the same energy in different species, as is the case here with, e.g., the ~100 eV and ~1000 eV bands evident in both H^+ and O^+ (and to a lesser extent, He^+) from ~02:00 to 02:09 UT. Therefore, the banding cannot be time-of-flight, velocity dispersion from a common source, as proposed by *Boehm et al.* [1999] and *Hirahara et al.* [1997] for their quiet time banding events. In addition, there is very little energy dispersion with latitude. There is no evidence for the energy band ratios predicted by either of the time-of-flight mechanisms discussed by *Boehm et al.* [1999].

Time-of-flight dispersion is sometimes visible in the distribution functions within an individual energy band. Figure 6 shows the ion distribution for the one second snapshot at 02:03:29–02:03:30 in two different formats: energy flux as a function of energy with pitch angle in color scale (Figure 6a) and energy flux as a function of pitch angle with energy in color scale (Figure 6b). There is dispersion evident in the relation between the pitch angles and the energy of particles within a given band at a given time. For example, the bands at ~20 eV and ~100 eV visible as peaks in Figure 6a have clear pitch angle dispersion, with the lower energy components (left section of the peak) having higher pitch angles (~123–134°; red and orange) and the higher energy components closer to perpendicular (~72–95°; blue and green).

Figure 7 shows energy spectrograms from the LANL-97A geosynchronous satellite during the time of the last orbits in Figures 2 and 3, when LANL-97A was on the dayside and in relatively close conjunction with FAST. The banded ions are evident in all look directions, but most prominently in the field-aligned directions (north and south), with clear energy dispersion. Fits to these dispersion curves do not directly match any of the

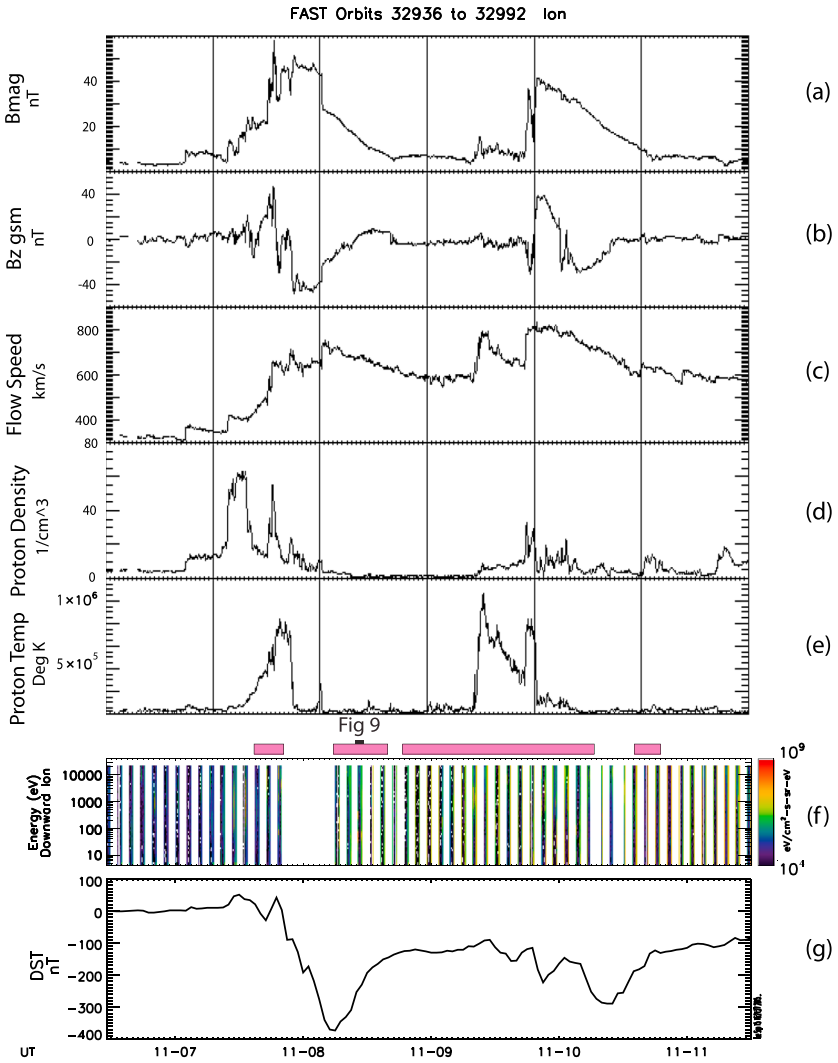

Figure 8. ACE magnetic field measurements of (a) magnitude of B (B_{mag}) and (b) north-south component of B (B_z); (c) solar wind proton speed, (d) temperature, and (e) density; (f) FAST ion spectrograms showing all times when FAST ion data were taken during the storm (the magenta bars above this panel represent orbits in which banded ions are observed; the black bar and "Figure 9" indicate the orbit which will be shown expanded in the subsequent figure); and (g) *Dst* level (from the Kyoto World Data Center for Geomagnetism) for the 5 day period from 06 November 2004 12:00 to 11 November 2004 12:00.

dispersion models, as we will discuss in detail later. Similar energy-dispersed ions are observed with the LANL satellites during most of the strong storms, often following sudden compressions of the magnetosphere. Particle injections in the equatorial plane may provide a source for the banded ions; potential source populations are being addressed in a separate study as discussed in section 7.

4. Case Studies of the November 2004, November 2003, and August 1998 Storms

Potential plasma sources, as well as energization and loss mechanisms, can be addressed by comparing the canonical observations obtained during the Halloween storm to observations from other large storms. The next two events occurred during the same season (end of October through end of November), the FAST orbital planes were similar, and southern hemisphere data were collected. There were, however, distinct differences observed in the time until the convection electric field penetrated to low L-shell, the density of the plasma sheet, and the strength of the initial shocks [*Mannucci et al*., 2008; *Abdu et al*., 2003].

The superstorm on 20–22 November 2003 had a several hour delay before the enhanced electric field penetrated to low L [*Mannucci et al*., 2008]. The plasma sheet as observed by the LANL geosynchronous satellites

was dense, reaching ~5 cm^{-3} at the time of minimum *SYM-H* [*Ebihara et al*., 2005]. In the underlying ionosphere, the subauroral electron temperature peak observed by DMSP reached ~10,000 K but only after the prompt penetration electric field appeared and soft energy-banded ions drifted onto these field lines. In contrast, the November 2004 case had no delay in the electric field penetration [*Mannucci et al*., 2008]. In fact, the largest vertical plasma drifts due to a prompt penetration electric field ever recorded over Jicamarca occurred during this event [*Fejer et al*., 2007]. The nightside plasma sheet density observed by the LANL satellites near the times of minima in *SYM-H* was only ~1–2 cm^{-3}. The subauroral electron temperature peak was much weaker in this case. The August 1998 storm also featured a prompt penetration electric field [*Abdu et al*., 2003], as well as observations of strong ULF waves which are thought to have produced the fast buildup of the electron radiation belts and slow buildup of the inner proton belt that occurred during this storm [*Hudson et al*., 2001]. These distinctions between the environments, in which the energy-banded ions were produced, can offer constraints on potential source mechanisms, although it is well beyond the scope of this paper. A study of the much larger set of moderate storms is now underway, and comparing the environmental conditions during those storms, especially those where the bands are not present, to those presented in this study will hopefully allow us to determine the generation mechanism(s) responsible for the ion bands, as discussed in section 7.

4.1. 6–11 November 2004

The 7–11 November 2004 storm is shown in Figure 8 in the same format as Figure 1, with the addition of ACE solar wind proton speed, density, and temperature to the ACE magnetometer data, FAST ion data, and *Dst*. This storm actually consists of two separate storms, and the two shock fronts of the storms are evidenced by sharp rises in B_{mag} (Figure 8a) at ~18:00 UT on 7 and 9 November. This is followed by southward IMF B_z (Figure 8b), which lasts for ~12 h after each shock before turning northward (though after the second shock hits there is a brief southward period and then a longer northward period before the true southward turning). These two storms are also evident as large drops in the *Dst* index (Figure 8g), reaching ~ −370 after the first shock and ~ −290 after the second. This storm interval was associated with solar wind speeds of ~800 km/s (Figure 8c), not nearly as fast as in the Halloween storms but typical of strong geomagnetic storms. The FAST data show banded ions seen in almost every orbit throughout the main and recovery phases of the storm (indicated again by magenta bars above the FAST data; Figure 8f).

Note that the bands are present even at the onset of the storm (first magenta bar), which is occasionally but not generally observed. However, the exact time the bands are first observed within a given event is somewhat subjective. In this case, as with any time the bands are present at onset, the ions prior to the storm are very weak, structured but not necessarily banded at constant energy in the way the storm time bands are, present in only the H^+ in single loss cone distributions, and confined to a narrow, higher-latitude range. This is consistent with the quiet time H^+ bands observed by *Yao et al*. [2008]. Only after the onset of the storm (or after the arrival of the penetration electric field if it is delayed, as evidenced in the next example) does the bands intensify, expand to include O^+ and He^+, and extend to lower latitudes. This can happen somewhat gradually, again leading to a bit of subjectivity in determining when the bands "turn on," but the timing of the first magenta bar in this and all figures of this type indicates a time when the ions are clearly observed to be this new type of storm time ion bands.

Figure 9 shows FAST data from 08:48 to 09:04 UT on 8 November 2004, taken over ILAT from 63.9 to 47.3° south, MLT 7.3–8.5, and altitude ~3400–3800 km during the main phase, when *Dst* was ~ −320 nT and solar wind speed was ~650 km/s. Note that this is the next auroral zone crossing after the interval shown in Figure 1 of *Colpitts et al*. [2012]. The top four panels plot, respectively, the perpendicular ion energy flux from 4 to 30,000 eV, the downgoing ion energy flux, and the ion pitch angle distributions over two different energy ranges, 10–300 eV and 300–10,000 eV.

As in previous figures (Figures 2–4), banded ions are prominent in the top two panels and last from ~8:50 to 9:03 UT. They are distinct from the wedge-type dispersion [*Ebihara et al*., 2001] or storm time ring current ions described by *McFadden et al*. [2001], which are also evident at the higher energies and lower latitudes. The two different phenomena can co-occur, as in this event, as well as other days presented herein (see Figure 12). Consistent with the banding events shown above, the ion fluxes peak in the perpendicular direction, and there is little or no upgoing flux. The pitch angle distribution can be seen in more detail in the third and fourth panels: there is a double loss cone at the higher energies and a single loss cone at lower energies.

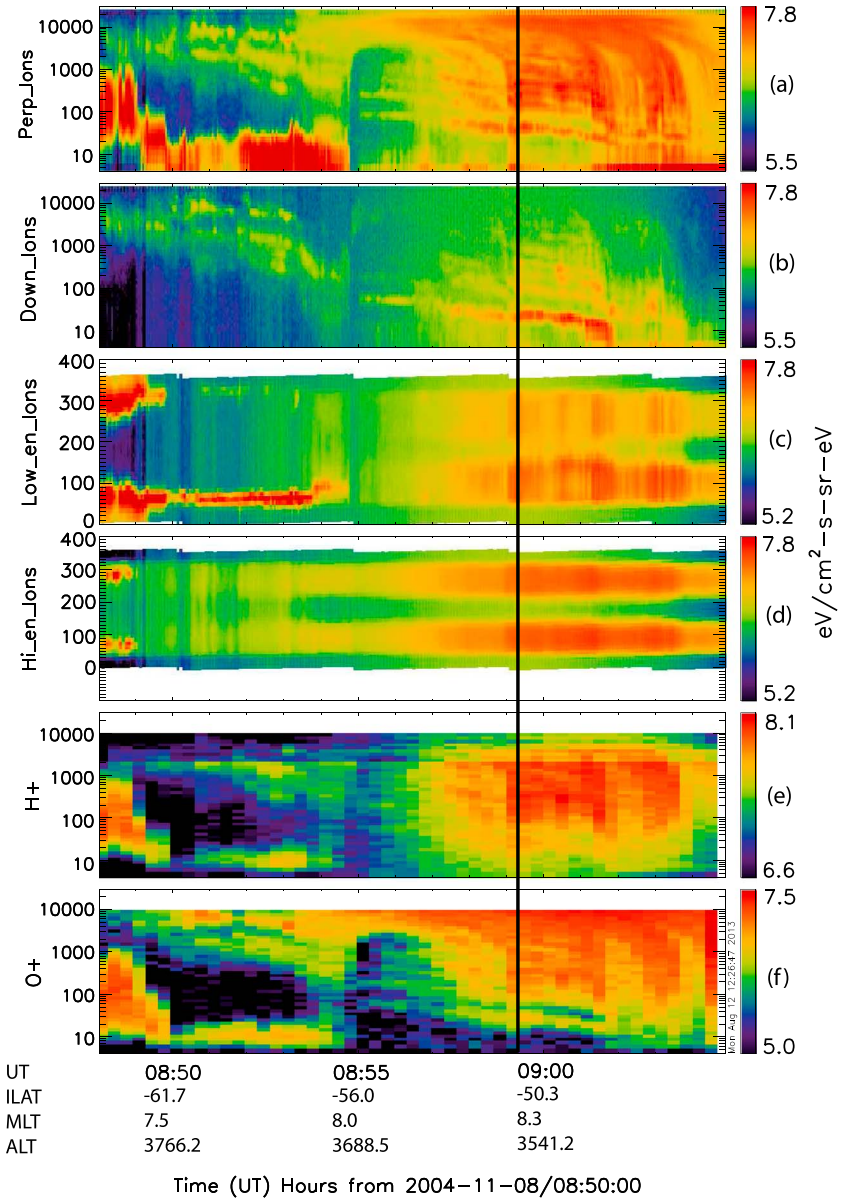

Figure 9. FAST (a) perpendicular and (b) downgoing ion energy spectrograms, (c) low-energy (10–300 eV) and (d) high-energy (300–10,000 eV) pitch angle spectrograms, and (e) H^+ and (f) O^+ ion energy spectrograms from 08:48 to 09:04 UT on 8 November 2004, taken over ILAT from 63.9 to 47.3° south, MLT 7.3–8.5 and altitude ~3400–3800 km. The black vertical line indicates time of data shown in Figure 10.

This pitch angle structure of the ion bands is illustrated more clearly in Figure 10a, which shows the energy flux distribution of all species of ions at ~08:59:17 (indicated by the black vertical line in Figure 9). The bands are clearly visible in the ion distribution, including both single loss cone bands at lower energies and double loss cone bands at higher energies. Figure 10b shows the ion energy flux distribution for ~02:03:30 on 31 October 2003, during the Halloween storms and at a time (marked by a vertical black line in Figure 5) within Figures 2, 3, and 5. In this case there is a clear single loss cone at lower energies, and at higher energies there is still a single loss cone, but the downgoing flux is considerably less than in the perpendicular direction.

Figures 9e and 9f show the energy flux of H^+ and O^+ ions, using the TEAMS ion mass spectrometer data. Note that the color scales are different in each panel. Ion bands are observed in both species, with several bands visible at the same energies in both species, particularly the lower energy bands (~20–300 eV) as well as some

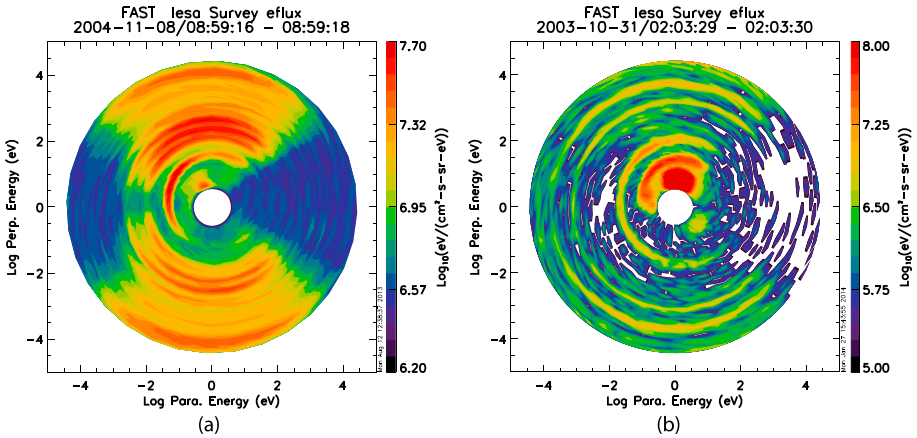

Figure 10. Energy flux distribution of all species of ions at (a) ~08:59:17 on November 8, 2004 (indicated by the black vertical line in Figure 9), and (b) ~02:03:30 on October 31, 2003 (marked by a vertical black line in Figure 5), with the log of the parallel energy on the *x* axis and perpendicular energy on the *y* axis.

higher energy bands. This storm event displays many of the signature features that were also clear in the figures showing the warm ions during other storms and described above: low-energy ions tend to extend to lower latitudes, bands occur for multiple orbits (tens of hours) and are more prominent on the dawnside, and the existence of oxygen and hydrogen bands at the same energies is not consistent with previously described mechanisms [*Boehm et al*., 1999; *Hirahara et al*., 1997]. The observation of both H^+ and O^+ at these low latitudes and with double loss cones at higher energies is also in contrast to the quiet time observations of *Yao et al*. [2008], who observed H^+ at higher latitudes and with single loss cones only.

4.2. 20–22 November 2003

The 20–22 November 2003 storm differs from the other storms investigated here in that the penetration electric field is delayed by several hours. This feature can potentially offer insight into the formation of the bands. Figure 11 shows an overview of the storm in the same format as Figure 8. The shock front of the storm is evident at ~08:30 as a sharp rise in B_{mag} (Figure 11a), as well as in proton flow speed, density, and temperature (Figures 11c–11e). A few hours later, B_z (Figures 11b) drops below zero (southward IMF) and remains southward for ~12 h. The *Dst* (Figure 11g) drops to −422 nT, making this the strongest storm of the last solar cycle by this measure, but the solar wind flow speed (Figure 11c) only reaches a moderate level of ~780 km/s.

Figure 12 shows perpendicular ion spectra from 12 consecutive dayside (MLT ~ 06:00–12:00) passes near the beginning of this storm (onset occurs at ~11:22 UT [*Mannucci et al*., 2008], between the third and fourth panels on the left, orbits 28997 and 28998). The six panels on the left are observed before the penetration electric field is established (~18:00 UT as determined from a combination of total electron content, vertical $E \times B$ drift, and interplanetary electric field E_y [*Mannucci et al*., 2008]), while the panels on the right occur afterward. The bands are already evident in the first orbit (28995; Figure 12, top left), before the onset of the storm, although they are weak and confined to a narrow latitude range. Around the time when the penetration electric field arrives (orbits 29000 and 29001), the bands move to considerably lower latitude (~50–60° as opposed to ~60–70° both before and after), as do the cusp injections visible in orbits 28998–29001. Note that the banded ions are present throughout the interval, both before and after the electric field penetrates. As can be seen in Figure 11 (magenta bars above the sixth panel), the banded ions are observed throughout the main and recovery phases of the storm as well.

4.3. 26–31 August 1998

The geomagnetic storm of 26–31 August 1998 provides another illustrative example of the banded ions, in particular highlighting the presence of the bands at the same energies in different ion species and the coincidence of the bands with frequency-banded electromagnetic waves. Figure 13 gives an overview of this storm in the same format as Figure 8. The initial shock front is visible in the B_{mag} data (Figure 13a) at 7:00 UT on 26 August, and it is followed after ~16 h by extended southward IMF B_z (Figure 13b) lasting ~24 h with

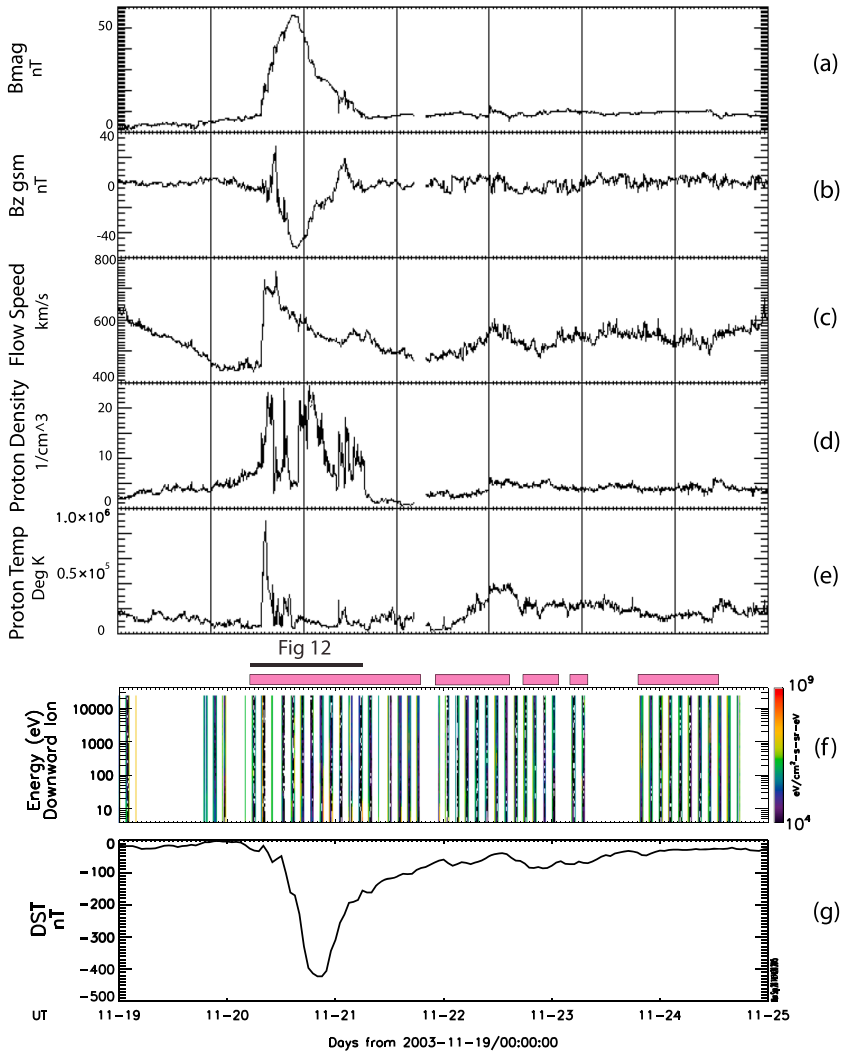

Figure 11. ACE magnetic field measurements of (a) magnitude of B (B_{mag}) and (b) north-south component of B (B_z); (c) solar wind proton speed, (d) temperature, and (e) density; (f) FAST ion spectrograms showing all times when FAST ion data were taken during the storm (the magenta bars above this panel represent orbits in which banded ions are observed; the black bar and "Figure 12" indicate the orbits which will be shown expanded in the subsequent figure); and (g) *Dst* level (from the Kyoto World Data Center for Geomagnetism) for the 6 day period from 19–25 November 2003.

a brief northward turning during that time. The solar wind speed (Figure 13c) drops off quickly over this time, from ~880 to ~520 km/s, typical values for storm time and quiet time solar wind speed. The *Dst* (Figure 13g) drops from ~30 to ~ −155, indicating a sizable storm, and FAST banded ions are observed throughout the main and recovery phases of the storm.

Figure 14 shows FAST data from 05:06 to 05:11 UT (MLT 2.2–2.3, ILAT 70.4-–4.1) on 30 August 1998 (during the recovery phase of the storm in the auroral zone, ~ 3 days after the peak *Dst* of −155 nT, with *Dst* ~ −50 nT, and solar wind speed ~570 km/s), in the same format as Figure 9 but with the flux of He^+ ions added in Figure 14g. There is very little flux in the downgoing component (Figure 14b), with only the lowest energy band evident with low flux, perhaps because the lowest energy bands are higher (>1000 eV) than in the case shown in Figure 9 (~20 eV). This is also evident in the low- and high-energy pitch angle plots (Figures 14c and 14d), where the low-energy plot in this case covers 4–2000 eV (high-energy 2000–30,000) and the downgoing loss cone is partially filled in at low energies and empty at high energies. As in the case shown in Figure 5, several energy bands are visible in the H^+, O^+, and He^+ populations at the same energies (in particular ~2000 and ~5000 eV from 05:07:15 to 05:07:45, ~1000 and ~2000 eV from 05:08:30 to 05:10:30), ruling out time of flight mechanisms for the generation of the bands.

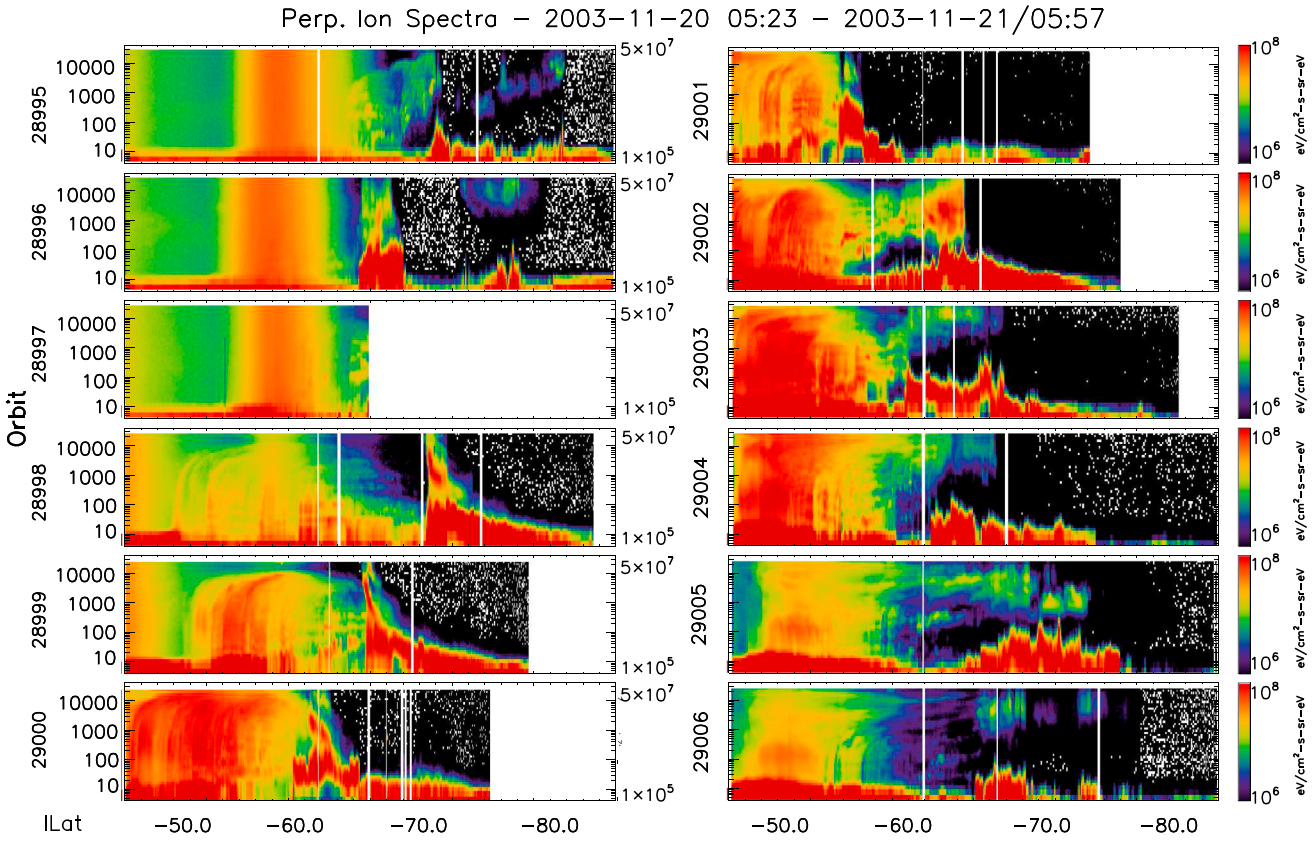

Figure 12. Perpendicular ion spectra from 12 consecutive dayside (MLT ~ 06:00–12:00) passes, covering the time period 05:23 on 20 November 20 to 05:57 on 21 November 2003, with latitude from 45 to 85° on the *x* axis.

Strong VLF emissions with frequencies from ~700 to 2000 Hz were observed in association with this storm (see Figure 5 in *Colpitts et al*. [2012], which shows the waves and the ions for the FAST pass just before the one in Figure 9). For this storm, the banded waves are not located significantly equatorward of the primary auroral electrons as in the other storms, and in fact, throughout this storm the banded waves and ions are observed more in the central auroral region than on the equatorward edge or subauroral region where they are typically observed. This could be related to the fact that this is not a superstorm; it is the weakest (minimum *Dst* −155) of the storms shown here and one of the weaker storms in which the banded ions have been observed to date. This can be seen in Table 1, which lists the storms investigated for this study chronologically, as well as the minimum *Dst*, presence of banded ions (Y meaning yes for all), and presence of banded waves (Y again being yes, P being possible/partial, N/A reflecting the lack of available wave data, green shading representing FAST wave data, and yellow shading DEMETER data). In fact, the interval shown here is a time of rapidly fluctuating north-south IMF and recurrent auroral activity. It is most likely a high-speed stream interval following behind the CME that initiated the magnetic storm. The auroral activity generated by the fluctuating IMF prolongs the recovery phase of the storm in *Dst*.

The close connection between the occurrence of waves and of banded ions for strong storms (minimum *Dst* −150 nT for FAST field data, −100 nT for DEMETER) when wave data were available on either DEMETER or FAST is presented in Table 1. Unlike the long-lived ion bands, the banded waves typically persist for only on the order of a few minutes and are seen during times when the ion density peaks, though there does not appear to be a consistent density threshold that is conditional for the wave observations. Details on the possible causal connections between the waves and ions are explored in *Colpitts et al*. [2012].

5. Statistical Occurrence

The warm energy-banded ions were observed in all 24 very large ($Dst < -150$ nT) storms encountered by the FAST satellite from May 1998 to December 2006 (see Table 1), and an additional 13 large ($Dst < -100$ nT) storms

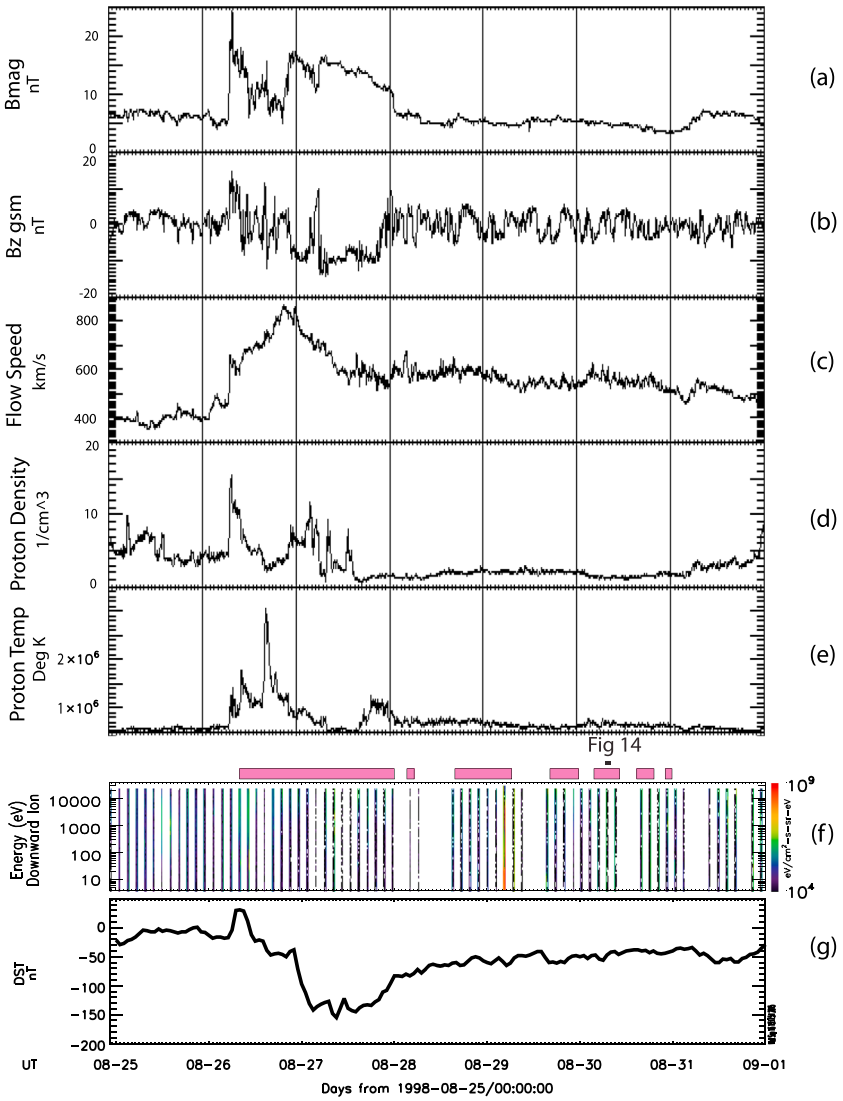

Figure 13. ACE magnetic field measurements of (a) magnitude of B (B_{mag}) and (b) north-south component of B (B_z); (c) solar wind proton speed, (d) temperature, and (e) density; (f) FAST ion spectrograms showing all times when FAST ion data were taken during the storm (the magenta bars above this panel represent orbits in which banded ions are observed; the black bar and "Figure 14" indicate the orbit which will be shown expanded in the subsequent figure); and (g) *Dst* level (from the Kyoto World Data Center for Geomagnetism) for the 7 day period from 25 August to 01 September 1998.

added to the study to take advantage of the DEMETER satellite to investigate banded waves coincident with the banded ions [*Colpitts et al.*, 2012]. A banded ion event was identified when banded ions were observed in any region from the auroral zone to deep within the plasmasphere. It was not required that all elements of the complex phenomenology during superstorms including the penetration of ions to extremely low latitudes and the overlap with wedge-type ions deep within the plasmasphere be present for an event to be identified. Thus, the statistical study focuses on banded ions alone and the conditions under which they appear throughout the auroral and subauroral regions. Since banded ions are observed during virtually all levels of magnetic activity [cf. *Yao et al.*, 2008] in the diffuse auroral region, the intensity of storms during which they occur is extended to include large and some moderate storms as well. A more rigorous statistical study incorporating all moderate storms is beyond the scope of this paper but is planned for the near future and discussed in section 7.

The banded ions were observed in both the northern and southern hemispheres, on the dayside and the nightside, though the dayside observations tend to be more constant in energy, while on the nightside the bands are more typically dispersed in energy and latitude, with higher energies observed at higher

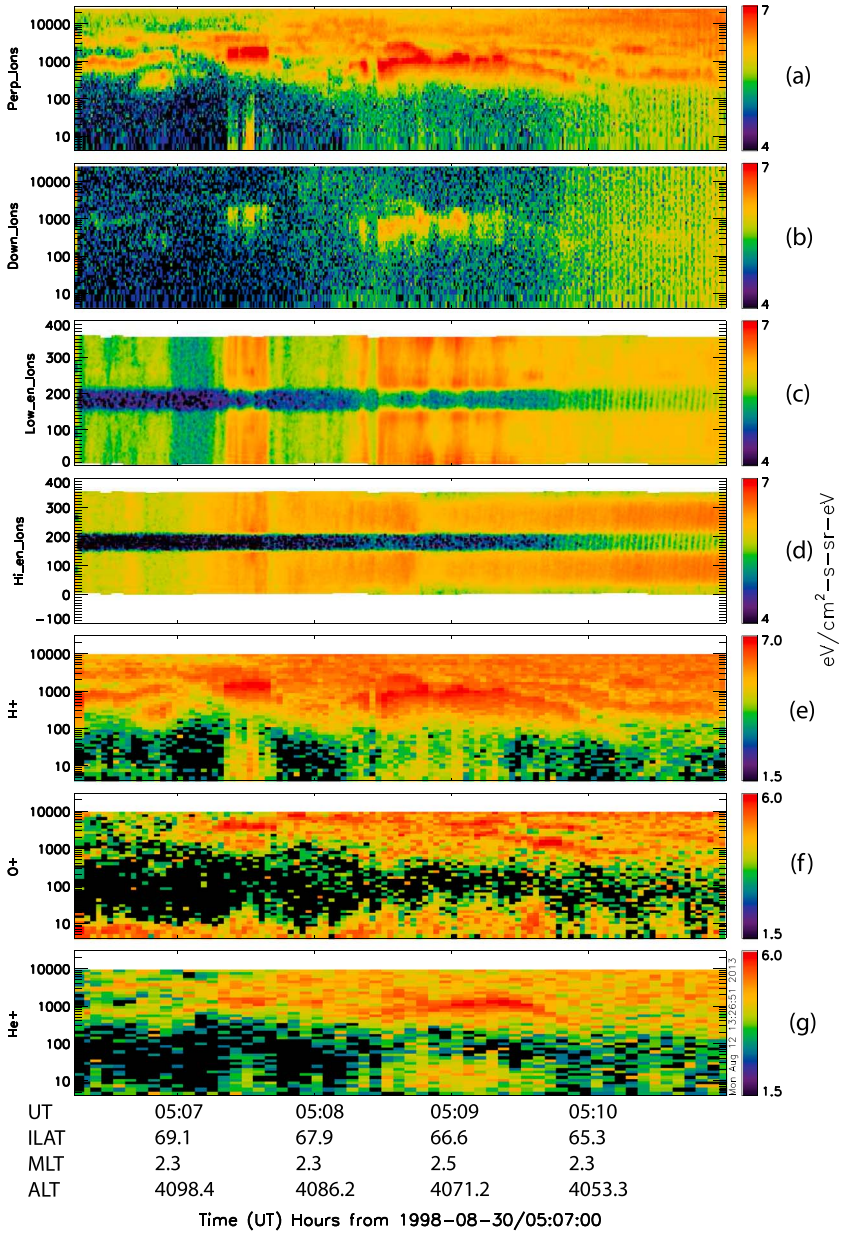

Figure 14. FAST (a) perpendicular and (b) downgoing ion energy spectrograms; (c) low-energy (10–300 eV) and (d) high-energy (300–10,000 eV) pitch angle spectrograms; and (e) H^+, (f) O^+, and (g) He^+ ion energy spectrograms from 05:06 to 05:11 UT on 30 August 1998 (MLT 2.2–2.3, ILAT 70.4–64.1).

latitudes. The bands occurred throughout the main and recovery phases of the storms, at all local times MLT 00:00–24:00, all FAST altitudes ~350–4175 km, and geomagnetic latitudes ranging from 45 to 85°, extending to the lower latitudes during the main phase and higher latitudes during the recovery phase. Due to data rate and contact time with and availability of antennae, we did not always receive data from both the nightside and dayside (and northern and southern) portion of an orbit over the desired 45:00–90:00 MLAT range, accounting for many of the passes where the bands were not observed, but over the data set of storms all MLT and latitude are covered. The bands were observed coincident with frequency-banded waves during some intervals of each storm on either FAST or DEMETER in all 27 storms where wave data exist.

The observation of banded warm ions during storms with intensity < -100 nT is consistent with the results of *Huang et al.* [2005]. They identified significant soft ion precipitation in DMSP observations at subauroral latitudes extending to as low as 33° (but more typically to 40°) during all storms with minimum $Dst < -200$ nT

Table 1. List of Large Geomagnetic Storms Investigated[a]

Date	Min *Dst*	Banded Ions	Banded Waves
03–07/05/98	−205	Y	Y
26–31/08/98	−155	Y	Y
25–26/09/98	−207	Y	Y
22–24/09/99	−173	Y	Y
22–25/10/99	−237	Y	Y
06–08/04/00	−288	Y	Y
15–17/07/00	−301	Y	P
12–14/08/00	−235	Y	P
17–19/09/00	−201	Y	Y
04–06/10/00	−182	Y	Y
06–07/11/00	−159	Y	Y
31/03–01/04/01	−387	Y	N/A
11–12/04/01	−271	Y	N/A
21–25/10/01	−187	Y	N/A
27–31/10/01	−157	Y	N/A
06–07/11/01	−292	Y	N/A
17–19/04/02	−127	Y	N/A
19–21/04/02	−149	Y	N/A
29–30/10/03	−353	Y	N/A
30–31/10/03	−383	Y	N/A
20–21/11/03	−422	Y	N/A
26–30/07/04	−197	Y	Y
30–31/08/04	−126	Y	Y
07–08/11/04	−373	Y	Y
09–10/11/04	−289	Y	Y
18–20/01/05	−121	Y	P
21–23/01/05	−105	Y	Y
08–10/05/05	−127	Y	P
15–19/05/05	−263	Y	Y
20–22/05/05	−103	Y	Y
30–31/05/05	−138	Y	Y
12–13/06/05	−106	Y	Y
24–26/08/05	−216	Y	Y
31/08–03/09/05	−131	Y	Y
11–12/09/05	−147	Y	Y
14–15/04/06	−111	Y	Y
15–16/12/06	−146	Y	Y

[a]Date, minimum *Dst*, and presence of banded ions and banded waves are indicated. "P" indicates possible, but not clear, presence of banded waves; green shading represents FAST wave data; yellow shading represents DEMETER data; and "N/A" indicates no wave data available on FAST or DEMETER.

(roughly superstorm intensity). In contrast, they found weak warm ion precipitation for storms with minimum *Dst* in the range of −100 to −150 nT but only if the main phase lasted for several hours. They did not investigate in detail the occurrence of energy bands within this precipitating component.

The typical energy range of the ion bands is 100–10,000 eV, but the observed energies extend from ~10 to 25,000 eV. Observed ion densities were typically 1–2 cm^{-3} but extended from 0.5 to 5.0 cm^{-3}. The bands are typically roughly constant in energy, aside from the occasional nightside dispersion mentioned previously. Bands are often evident in all component species (H^+, He^+, and O^+), and often all at the same energies, with energy flux ratio $O^+/H^+ \sim 0.1$–2.0. The flux peaks in the perpendicular, or trapped population, and can have a single loss cone distribution with the bands visible in both the downgoing and perpendicular components or double loss cone distribution with bands only in ions with perpendicular pitch angles. The single loss cone is more common for the lower energy bands, but the distribution is uncorrelated with altitude, latitude, MLT, or storm phase, unlike in previous reports of banded ions such as *Yao et al.* [2008], which was restricted to the year 2000, where a single loss cone distribution was observed for the quiet time H^+ bands and a double loss cone for storm time O^+ bands.

6. Test of Models for the Origin of the Bands Using Geosynchronous Data

During some of the events studied, including the Halloween storms, the LANL geosynchronous satellites observed broad regions of energy dispersed field-aligned ions from ~100 eV to 40 keV. The ions occurred primarily on the dayside and often in association with strong magnetospheric compressions (inside geosynchronous). The simultaneous observation of dispersed banded ions at geosynchronous orbit and the energy banded ions at low altitudes provides the opportunity to test various models for the sources of and mechanisms producing the energy-banded ions at low altitudes, as well as the dispersed ions at geosynchronous. The two sources usually invoked are equatorial (for example, substorm injection on the nightside) and ionospheric (for example, outflow from the polar cap boundary). The energy dispersion is interpreted as being due to time of flight from the source region, in combination with subsequent bounce motion along the magnetic field.

Useful times for the comparison include the bounce period, which for 1 keV H^+ is ~300 s and for 1 keV O^+ is ~1200s. Historically, the typical cutoff when modeling and observing particle transport in this region of the magnetosphere is that grad B dominates for energies >100 keV and $E \times B$ for energies <30 keV, with some

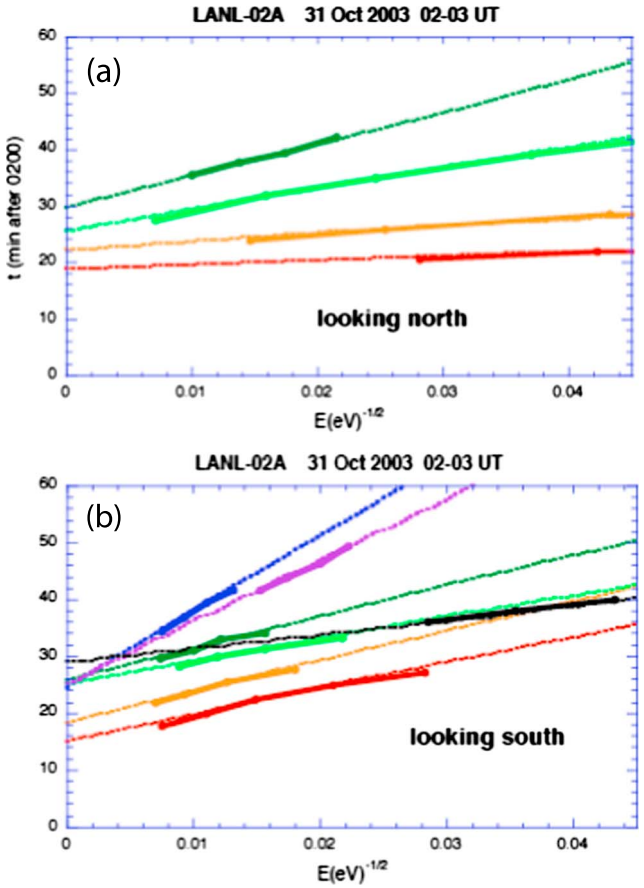

Figure 15. Time (in minutes after 02:00 UT on 31 October 2003) versus $1/E^{1/2}$ plots for a subset of the LANL 02A ion band observations (thick lines) shown in Figure 7, with linear fits to each band shown underlying the observations, for (a) north and (b) south looking directions.

overlap of the two processes in the intermediate 30–100 keV range [*Schulz and Lanzerotti*, 1974; *Sheldon and Gaffey*, 1993]. *McFadden et al.* [2001] used FAST data to establish a cutoff at ~5–10 keV as the region below which grad B is not effective at FAST locations. At the energies and L-shells of the FAST observations shown here, there is no doubt that the particles are $E \times B$ drifting eastward, and not grad B drifting westward, so grad-B and curvature drift effects cannot be responsible for the observed banding. At the LANL spacecraft location, there is some grad-B contribution at the highest energies, but as the bands are dispersed down to ~100 eV the grad-B drift cannot explain the dispersion. For L ~ 6–10, only ions with $E >$ ~1.5 keV will have a large contribution to their motion due to the grad B drift; for lower energies, co-rotation dominates. The energy dispersion observed by the LANL satellites was compared to that expected from time of flight. The relationship between the energy, E; time of observation, t; time of injection, t_0; and source distance, S, is given by

$$E(t) = 1/2m_i\left[S/(t-t_0\right]^2 \quad (1)$$

or defined for t

$$t - t_0 = S[m/2E]^{1/2} \quad (2)$$

For dispersion due to bounce motion along the magnetic field, the source distance depends on multiples of the field-line length and whether the source (observation point) is equatorial (ionospheric). When both the source and observation points are the same location, the energy will depend on n^2 (n = 1,2,3…bounce number); when they are different the energy depends on $[(2n \times 1)/2]^2$. Figure 15 shows the time (in minutes after 02:00 UT on 31 October 2003) versus $1/E^{1/2}$ plots for a subset of the LANL 02A ion band observations (thick lines), with linear fits to each band shown underlying the observations. All of the bands observed in both the north (Figure 15a) and south looking (Figure 15b) directions show the expected linear relationship for time-of-flight effects. The slopes of the bands from the linear fits shown in Figure 15, as well as those observed with another LANL satellite (97A), are plotted in Figure 16 (along with the calculated errors in the fits) for comparison with the slopes expected for an ionospheric source (S = l/2, 2 l/2, 5 l/2…) or an equatorial source (S = l, 2 l, 3 l…), where l is the length of the field line through the geosynchronous location. The assumed species are H^+ (Figure 16, top), He^+ (Figure 16, middle), and O^+ (Figure 16, bottom).

Although most of the ion bands fit a time-of-flight dispersion, in some cases it was for an ionospheric source and in some for an equatorial source [*Thomsen et al.*, 2004]. Note that for some bands, multiple bounces are required to fit the dispersion; however, not all the intermediate bounces are observed. In addition, multiple source injection times were necessary (t_0 in Figure 16). This is not inconsistent with the multiple magnetospheric compressions and/or the FAST observations of ionospheric outflow over a long interval. The tan shading in Figure 16 indicates some clustering in t_0, with most of the calculated slopes bunched around a few times. Preliminary analysis suggests that these times may be separated by roughly the period of ion *Pc*5 oscillations (~3–3.5 min), and *Pc*5 waves are often observed just after the magnetopause compressions

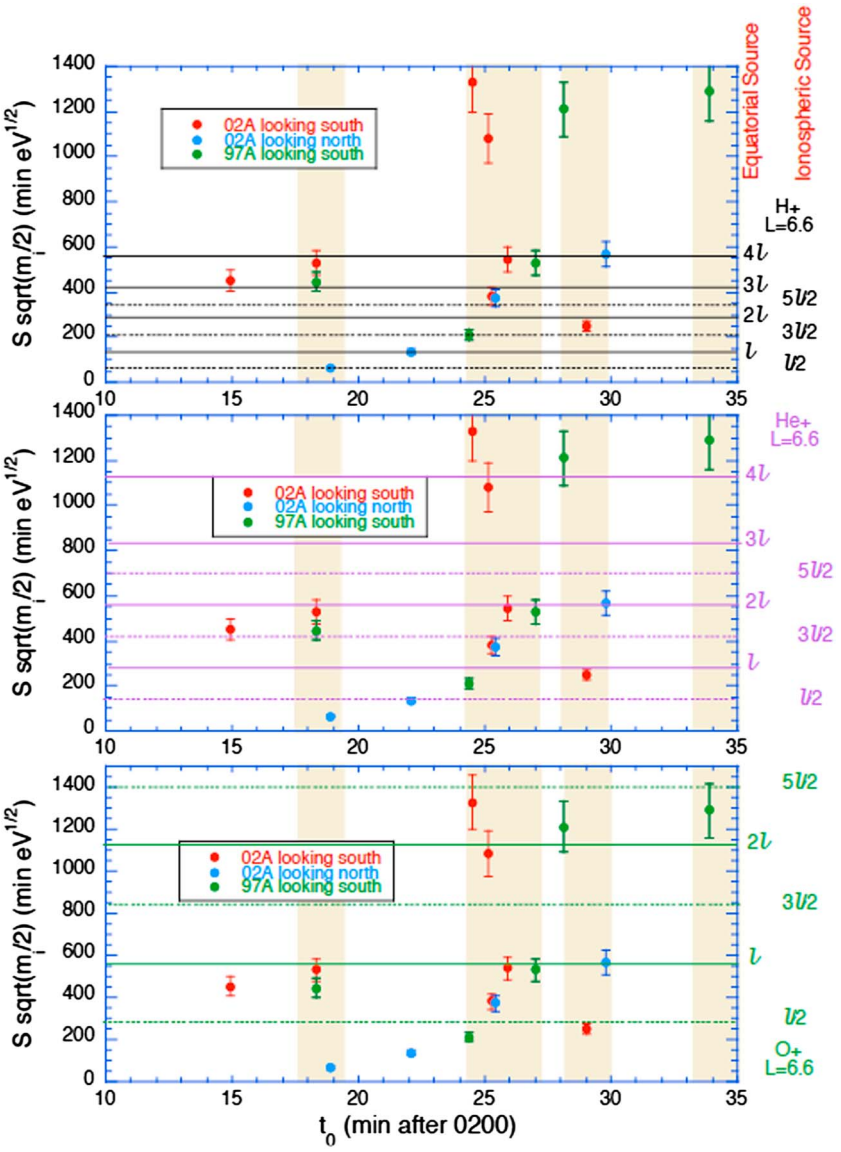

Figure 16. The slopes of the bands from the linear fits shown in Figure 16, as well as those observed with another LANL satellite (97A), (along with the calculated errors in the fits) for comparison with the slopes expected for an ionospheric source ($S = l/2, 2\,l/2, 5\,l/2,\ldots$) or an equatorial source ($S = l, 2\,l, 3\,l,\ldots$), where l is the length of the field line through the geosynchronous location. The assumed species are (top) H^+, (middle) He^+, and (bottom) O^+.

in these strong storms. This implies that *Pc*5 oscillations may play a role in the generation or modulation of these ion bands, but more investigation is required to determine the exact nature of the relationship between the bands and *Pc*5 waves.

7. Discussion and Conclusions

We observe energy-banded ions from tens to ten thousands of eV in the auroral and subauroral zones during every large (minimum $Dst < -150$ nT, in some cases < -100 nT) geomagnetic storm encountered by the FAST satellite. Intense bands with similar properties can persist for 12 h, as in the Halloween storm. Some degree of ion banding is seen throughout all of the storms, although some individual orbits do not display visible bands over the latitude range measured or during all magnetic local times observed. We observe multiple distinct bands (often >6), and the O^+, He^+, and H^+ bands are often observed at the same energies. During the times of banded ion observations, shorter periods of a new type of frequency-banded electromagnetic wave are also observed. In addition, long-lasting intervals of field-aligned energy-dispersed ions

from ~100 eV to 40 keV are seen in the LANL instruments onboard geosynchronous satellites for some of the events studied in detail. We find that the geosynchronous ions have energy dispersion consistent with time of flight, but without a consistent source region for all of the bands, and that the FAST bands only show such dispersion within an individual band and not across bands or latitude. The temporal spacing of the LANL observations appears to be somewhat consistent with the period of *Pc*5 oscillations. The relationship between this and the energy spacing in the FAST observations is unclear, but it is possible that *Pc*5 oscillations play a role in the generation or modulation of the ion bands. Investigation of the potential nature of the role of *Pc*5 oscillations is beyond the scope of this paper, but will be a part of the statistical study described below.

There have been several other independent observations of banded ions and investigations into the source regions and generation mechanisms of the bands; however, none of the observations or proposed generation mechanisms can explain the ion bands reported here. On the basis of the different ILAT and MLT dependence for O^+ and H^+ energy banded ions in a statistical study of ions observed by FAST, *Yao et al*. [2008] concluded that the O^+ and H^+ bands had different source mechanisms. They suggest that the H^+ ions are plasma sheet ions generated by impulsive particle injections due to pulsed dayside reconnection, while the O^+ ions are ionospheric and generated by convective transport. *Ebihara et al*. [2001] modeled three types of energy banding observed in Viking data referred to as wedge-like structures. The data were consistent with a generation mechanism that combined variable source density and location with time-dependent convection electric fields. Their "Type-1" banding is consistent with the energy dispersion we observe in some cases, in particular in the nightside and occasionally at the low latitude edge of the dayside energy-banded ions, where the ions increase in energy with increasing latitude.

These wedge-like structures cannot be produced by ion drifts alone but require particular spatial or temporal characteristics in the source population [*Ebihara et al*., 2001]. Type 1 (ordinary) patterns are produced by a source that is narrow in the radial direction and extended in the azimuthal direction described as azimuthal stripes. Simulations indicate that the wedge-like ions are formed most likely from a cold ion source (T ~100 eV) rather than the hot plasma sheet [*Ebihara et al*., 2001, 2008]. *Yamauchi et al*. [2009] speculate that the cold dense plasma sheet [cf. *Fujimoto et al*., 1997] or superdense plasma sheet intervals [*Borovsky et al*., 1997] are likely sources of the cold plasma for the Type 1 wedge-like ion structures. Another possible source is the impulsive electric field associated with substorms that is radially confined but azimuthally extended.

Utilizing a particle tracing code with an idealized storm time electric field model, *Huang et al*. [2005, 2007] examined possible source locations for low-energy precipitating ions observed by DMSP at low latitudes during major storms. Based on the observed separation between electrons and ions, they concluded that these ions must have a source inside the plasmasphere, not the plasma sheet, and were associated with the large and time-varying penetration electric fields. One of the events discussed was the Halloween storm. The advantage of DMSP is the fact that there are multiple spacecraft with the ability to simultaneously observe precipitating ions, the penetration electric field, and the electron temperature peaks; the disadvantage is that the bulk of the energy banded ions shown here are mirroring at higher altitudes and would not be evident in the precipitating component measured by DMSP.

The comparison of the FAST banded ions and the geosynchronous data during the Halloween storm provides evidence in the FAST data and the LANL data for an ionospheric source, as well as for a plasma sheet source. The LANL data show clear evidence for an equatorial dayside source associated with magnetospheric compressions, likely the boundary layer. The equatorial source observations are consistent with *Mauk* [1986] and *Quinn and McIlwain* [1979], as well as with the source characteristics inferred by *Boehm et al*. [1999]. Although the LANL data are consistent with time-of-flight dispersion, the FAST data do not appear to be since the O^+ and H^+ bands have the same energies (not velocities). There is no clear evidence for different sources for the O^+ (or He^+) bands than for the H^+ bands.

The banded ions are observed in all of the large storms encountered by the FAST satellite, but they are also observed in some more moderate (minimum $Dst \sim -100$ nT) storms. In particular, the 21 January 2005 storm had a minimum *Dst* of only −105 nT, but featured several phenomena typically associated with larger storms [*Kozyra et al*., 2013, 2014], including warm energy-banded ions similar to those reported herein, with multiple bands at the same energies observed in different components (H^+ and He^+ or H^+ and O^+). We are preparing additional studies of this fascinating storm, including the finding that the observed bands were consistent

with time-of-flight mechanisms from a localized source if we suppose a superposition of multiple bands formed by protons bouncing between mirror points combined with the time-of-flight separation of heavier ions (He^+ and O^+) arriving directly from the source. This type of mechanism would not explain the bands observed in the case studies shown here, where there are many bands with all three components at the same energies.

Another finding from this January 2005 storm is that the bands occurred on the dayside only during northward IMF conditions, and this together with other plasma characteristics allows us to infer that intermittent capture of low-latitude boundary layer plasma was the source for these banded ions. While in all of our case studies here the bands are observed in both northward and southward IMF conditions, this is an interesting additional source to be considered for these ions, combined with the ionospheric ion outflow, equatorial plasma, and substorm injections. In addition to the studies of this particular moderate event, we are beginning a study of the much larger subset of moderate storms encountered by FAST as well as quiet times, where we will determine in what percentage of moderate storms the ion bands are observed and if there is a threshold for how strong a storm must be for the bands to be present, or if there is some other factor besides minimum *Dst* which determines the presence of the bands. This study will also include statistical studies of the relative strength, number, and energy range of the bands in each component species as a function of storm phase, MLT, latitude, altitude, *Dst*, and other parameters as well as address potential source populations for the ion bands and should give us a clearer picture of how the banded ions are generated.

Acknowledgments

The FAST data used for the figures in this paper are available at http://sprg.ssl.berkeley.edu/fast/scienceprod/welcome.html. The Kyoto *Dst* data are available at http://wdc.kugi.kyoto-u.ac.jp/dstdir/index.html. The ACE solar wind data are available at http://www.srl.caltech.edu/ACE/ASC/. LANL MPA color spectrograms are available at http://www.mpa.lanl.gov/cgi-bin/search.cgi. M.F.T. is grateful to Los Alamos National Laboratory for support as a guest scientist. This work was supported by NASA grants NNX07AG37G, NNX12AJ53G, and NNX14AF32G.

References

Abdu, M. A., C. M. Denardini, J. H. A. Sobral, I. S. Batista, P. Muralikrishna, K. N. Iyer, O. Veliz, and E. R. Paula (2003), Equatorial electrojet 3-M irregularity dynamics during magnetic disturbances over Brazil: Results from the new VHF radar at São Luís, *J. Atmos. Sol. Terr. Phys.*, *65*, 1293–1308, doi:10.1016/j.jastp.2003.08.011.

Ashour-Abdalla, M., L. M. Zelenyi, J. M. Bosqued, and R. A. Kovrazhkin (1992), Precipitation of fast ion beams from the plasma sheet boundary layer, *Geophys. Res. Lett.*, *19*(6), 617–620, doi:10.1029/92GL00048.

Ashour-Abdalla, M., J. M. Bosqued, M. El-Alaoui, V. Peroomian, L. M. Zelenyi, R. J. Walker, and J. Wright (2005), A stochastic sea: The source of plasma sheet boundary layer ion structures observed by Cluster, *J. Geophys. Res.*, *110*, A12221, doi:10.1029/2005JA011183.

Baker, D. N., N. E. Turner, and T. I. Pulkkinen (2001), Energy transport and dissipation in the magnetosphere during geomagnetic storms, *J. Atmos. Sol. Terr. Phys.*, *63*(5), 421–429, doi:10.1016/S1364-6826(00)00169-3.

Bame, S. J., D. J. McComas, M. F. Thomsen, B. L. Barraclough, R. C. Elphic, J. P. Glore, J. T. Gosling, J. C. Chavez, E. P. Evans, and F. J. Wymer (1993), Magnetospheric plasma analyzer for spacecraft with constrained resources, *Rev. Sci. Instrum.*, *64*, 1026, doi:10.1063/1.1144173.

Bell, J. T., M. S. Gussenhoven, and E. G. Mullen (1997), Super storms, *J. Geophys. Res.*, *102*, 14,189–14,198, doi:10.1029/96JA03759.

Boehm, M., D. Klumpar, E. Möbius, L. Kistler, J. McFadden, C. Carlson, and R. Ergun (1999), FAST auroral snapshot observations of bouncing ion distributions: Fieldline length measurements, *J. Geophys. Res.*, *104*, 2343–2355, doi:10.1029/98JA02290.

Borovsky, J. E., M. F. Thomsen, and D. J. McComas (1997), The superdense plasma sheet: Plasmaspheric origin, solar wind origin, or ionospheric origin, *J. Geophys. Res.*, *102*, 22,089–22,106, doi:10.1029/97JA02469.

Bosqued, J. M., M. Ashour-Abdalla, M. El Alaoui, V. Peroomian, L. M. Zelenyi, and C. P. Escoubet (1993), Dispersed ion structures at the poleward edge of the auroral oval: Low-altitude observations and numerical modeling, *J. Geophys. Res.*, *98*(A11), 19,181–19,204, doi:10.1029/93JA01143.

Carlson, C. W., J. P. McFadden, P. Turin, D. W. Curtis, and A. Magoncelli (2001), The electron and ion plasma experiment for Fast, *Space Sci. Rev.*, *98*, 33–66.

Cattell, C. A., M. F. Thomsen, J. Kozyra, B. Lavraud, J. Borovsky, and J. Dombeck (2004), Eergized banded ions during large geomagnetic storms: Comparisons of observations at geosynchronous and low altitudes, COSPAR04-A-02925.

Colpitts, C. A., C. A. A. Cattell, J. U. Kozyra, and M. Parrot (2012), Satellite observations of banded VLF emissions in conjunction with energy-banded ions during very large geomagnetic storms, *J. Geophys. Res.*, A10211, doi:10.1029/2011JA017329.

Dombeck, J., C. Cattell, J. R. Wygant, A. Keiling, and J. Scudder (2005), Alfven waves and Poynting flux observed simultaneously by Polar and FAST in the plasma sheet boundary layer, *J. Geophys. Res.*, *110*, A12S90, doi:10.1029/2005JA011269.

Ebihara, Y., M. Yamauchi, H. Nilsson, R. Lundin, and M. Ejiri (2001), Wedge-like dispersion of subkeV ions: Particle simulation and Viking observation, *J. Geophys. Res.*, *106*, 29,571–29,584, doi:10.1029/2000JA000227.

Ebihara, Y., M. Ejiri, H. Nilsson, I. Sandahl, M. Grande, J. F. Fennell, J. L. Roeder, D. R. Weimer, and T. A. Fritz (2004), Multiple discrete-energy ion features in the inner magnetosphere: Event of February 9, 1998, *Ann. Geophys.*, *22*, 1297–1304, doi:10.5194/angeo-22-1297-2004.

Ebihara, Y., M.-C. Fok, S. Sazykin, M. F. Thomsen, M. R. Hairston, D. S. Evans, F. J. Rich, and M. Ejiri (2005), Ring current and the magnetosphere-ionosphere coupling during the superstorm of 20 November 2003, *J. Geophys. Res.*, *110*, A09S22, doi:10.1029/2004JA010924.

Ebihara, Y., L. M. Kistler, and L. Eliasson (2008), Imaging cold ions in the plasma sheet from the equator-S satellite, *Geophys. Res. Lett.*, *35*, L15103, doi:10.1029/2008GL034357.

Elphic, R. C., J. D. Means, R. C. Snare, R. J. Strangeway, L. Kepko, and R. E. Ergun (2001), Magnetic field instruments for the Fast Auroral Snapshot Explorer, *Space Sci. Rev.*, *98*, 151.

Ergun, R. E., et al. (2001), The FAST satellite fields instrument, *Space Sci. Rev.*, *98*, 67.

Fejer, B. G., J. W. Jensen, T. Kikuchi, M. A. Abdu, and J. L. Chau (2007), Equatorial ionospheric electric fields during the November 2004 magnetic storm, *J. Geophys. Res.*, *112*, A10304, doi:10.1029/2007JA012376.

Fennell, J. F., et al. (1998), Multiple discrete-energy ion features in the inner magnetosphere: Polar observations, *Phys. Space Plasmas*, *15*, 395.

Frahm, R. A., P. H. Reiff, J. D. Winningham, and J. L. Burch (1986), Banded ion morphology: Main and recovery storm phases, in *Ion Acceleration in the Magnetosphere and Ionosphere*, *Geophys. Monogr. Ser.*, vol. 38, edited by T. Chang et al., pp. 98–107, AGU, Washington, D. C.

Fujimoto, M., T. Terasawa, and T. Mukai (1997), The cold-dense plasma sheet: A Geotail perspective, *Space Sci. Rev.*, *80*, 325.

Gopalswamy, N., L. Barbieri, E. W. Cliver, G. Lu, S. P. Plunkett, and R. M. Skoug (2005), Introduction to violent Sun-Earth connection events of October–November 2003, *J. Geophys. Res.*, *110*, A09S00, doi:10.1029/2005JA011268.

Hamilton, D. C., G. Gloeckler, F. M. Ipavich, W. Stüdemann, B. Wilken, and G. Kremser (1988), Ring current development during the great geomagnetic storm of February 1986, *J. Geophys. Res.*, *93*(A12), 14,343–14,355, doi:10.1029/JA093iA12p14343.

Hirahara, M., A. Yamazaki, K. Seki, T. Mukai, E. Sagawa, N. Kaya, and H. Hayakawa (1997), Characteristics of downward flowing ion energy dispersions observed in the low-altitude central plasma sheet by Akebono and DMSP, *J. Geophys. Res.*, *102*(A3), 4821–4839, doi:10.1029/96JA03332.

Huang, C. Y., W. J. Burke, and C. S. Lin (2005), Ion precipitation in the dawn sector during geomagnetic storms, *J. Geophys. Res.*, *110*, A11213, doi:10.1029/2005JA011116.

Huang, C. Y., W. J. Burke, and C. S. Lin (2007), Low-energy ion precipitation during the Halloween storm, *J. Atmos. Sol. Terr. Phys.*, *69*, 101–108, doi:10.1016/j.jastp.2006.06.018.

Hudson, M. K., S. R. Elkington, J. G. Lyon, M. Wiltberger, and M. Lessard (2001), Radiation belt electron acceleration by ULF wave drift resonance: Simulation of 1997 and 1998 storms, *Geophys. Monogr. Ser.*, *125*, 289–296.

Klumpar, D. M., et al. (2001), The Time-of-Flight Energy, Angle, Mass Spectrograph (TEAMS) experiment for FAST, *Space Sci. Rev.*, *98*, 197.

Kovrazhkin, R. A., J. -A. Sauvaud, and D. C. Delcourt (1999), Interball-auroral observations of 0.1–12 keV ion gaps in the diffuse auroral zone, *Ann. Geophys.*, *17*, 734.

Kozyra, J. U., E. G. Shelley, R. H. Comfort, L. H. Brace, T. E. Cravens, and A. F. Nagy (1987), The role of ring current O^+ in the formation of stable auroral red arcs, *J. Geophys. Res.*, *92*(A7), 7487–7502, doi:10.1029/JA092iA07p07487.

Kozyra, J. U., M. O. Chandler, D. C. Hamilton, W. K. Peterson, D. M. Klumpar, D. W. Slater, M. J. Buonsanto, and H. C. Carlson (1993), The role of ring current nose events in producing SAR arc intensifications during the main phase: Observations during the September 19–24, 1984 Equinox Transition Study (ETS), *J. Geophys. Res.*, *98*, 9267–9283, doi:10.1029/92JA02554.

Kozyra, J. U., A. F. Nagy, and D. W. Slater (1997), The high altitude energy source for stable auroral red (SAR) arcs, *Rev. Geophys.*, *35*(2), 155–190, doi:10.1029/96RG03194.

Kozyra, J. U., et al. (2004), Coupling processes in the inner magnetosphere associated with midlatitude red auroras during superstorms, Eos Trans. AGU, 85(47), Fall Meet. Suppl., SM12B-03 INVITED.

Kozyra, J. U., W. B. Manchester IV, C. P. Escoubet, S. T. Lepri, M. W. Liemohn, W. D. Gonzalez, M. W. Thomsen, and B. T. Tsurutani (2013), Earth's collision with a solar filament on 21 January 2005: Overview, *J. Geophys. Res. Space Physics*, *118*, 5967–5978, doi:10.1002/jgra.50567.

Kozyra, J. U., et al. (2014), Solar filament impact on 21 January 2005: Geospace consequences, *J. Geophys. Res. Space Physics*, *119*, 5401–5448, doi:10.1002/2013JA019748.

Li, X., D. N. Baker, M. Temerin, W. K. Peterson, and J. F. Fennell (2000), Multiple discrete-energy ion features in the inner magnetosphere: Observations and Simulations, *J. Geophys. Res.*, *27*, 1447–1450, doi:10.1029/1999GL010745.

Mac-Mahon, R. M., and W. D. Gonzalez (1997), Energetics during the main phase of geomagnetic superstorms, *J. Geophys. Res.*, *102*(A7), 14,199–14,207, doi:10.1029/97JA01151.

Mannucci, A. J., B. T. Tsurutani, M. A. Abdu, W. D. Gonzalez, A. Komjathy, E. Echer, B. A. Iijima, G. Crowley, and D. Anderson (2008), Superposed epoch analysis of the dayside ionospheric response to four intense geomagnetic storms, *J. Geophys. Res.*, *113*, A00A02, doi:10.1029/2007JA012732.

Mauk, B. H. (1986), Quantitative modeling of the 'convection surge' mechanism of ion acceleration, *J. Geophys. Res.*, *91*, 13,423–13,431, doi:10.1029/JA091iA12p13423.

McComas, D. J., S. J. Bame, P. Parker, W. C. Feldman, J. L. Phillips, P. Riley, and J. W. Griffey (1999), Solar Wind Electron Proton Alpha Monitor (SWEPAM) for the Advanced Composition Explorer, *Space Sci. Rev.*, *86*, 563, doi:10.1023/A:1005040232597.

McFadden, J. P., Y. K. Tung, C. W. Carlson, R. J. Strangeway, E. Moebius, and L. M. Kistler (2001), FAST observations of ion outflow associated with magnetic storms, in *Space Weather*, *Geophys. Monogr. Ser.*, vol. 125, edited by P. Song, H. J. Singer, and G. L. Siscoe, pp. 413–421, AGU, Washington, D. C., doi:10.1029/GM125p0413.

Moore, T. E., W. K. Peterson, C. T. Russell, M. O. Chandler, M. R. Collier, H. L. Collin, P. D. Craven, R. Fitzenreiter, B. L. Giles, and C. J. Pollock (1999), Ionospheric mass ejection in response to a CME, *Geophys. Res. Lett.*, *26*, 2339–2342, doi:10.1029/1999GL900456.

Nakajima, A., K. Shiokawa, K. Seki, R. J. Strangeway, J. P. McFadden, and C. W. Carlson (2007), Particle and field characteristics of broadband electrons observed by the FAST satellite during a geomagnetic storm, *J. Geophys. Res.*, *112*, A06220, doi:10.1029/2006JA012184.

Parrot, M., A. Buzzi, O. Santolík, J. J. Berthelier, J. A. Sauvaud, and J. P. Lebreton (2006), New observations of electromagnetic harmonic ELF emissions in the ionosphere by the DEMETER satellite during large magnetic storms, *J. Geophys. Res.*, *111*, A08301, doi:10.1029/2005JA011583.

Peterson, W. K., K. J. Trattner, O. W. Lennartsson, H. L. Collin, D. N. Baker, T. I. Pulkkinen, P. K. Toivanen, T. A. Fritz, J. F. Fennell, and J. L. Roeder (1998), *Imaging the Plasma Sheet With Energetic Ions from the Polar Satellite*, *Proc. of ICS-4*, 813 pp., Terra Sci., Tokyo.

Quinn, J. M., and C. E. McIlwain (1979), Bouncing ion clusters in the Earth's magnetosphere, *J. Geophys. Res.*, *84*, 7365–7370, doi:10.1029/JA084iA12p07365.

Schulz, M., and L. J. Lanzerotti (1974), *Particle Diffusion in the Radiation Belts*, Springer, New York.

Sheldon, R. B., and J. D. Gaffey Jr. (1993), Particle tracing in the magnetosphere: New algorithms and results, *Geophys. Res. Lett.*, *20*, 767–770, doi:10.1029/93GL00835.

Shiokawa, K., K. Yumoto, C.-I. Meng, and G. Reeves (1996), Broadband electrons observed by the DMSP satellites during storm-time substorms, *Geophys. Res. Lett.*, *23*(18), 2529–2532, doi:10.1029/96GL01955.

Shiokawa, K., C.-I. Meng, G. D. Reeves, F. J. Rich, and K. Yumoto (1997), A multievent study of broadband electrons observed by the DMSP satellites and their relation to red aurora observed at midlatitude stations, *J. Geophys. Res.*, *102*(A7), 14,237–14,253, doi:10.1029/97JA00741.

Skoug, R. M., J. T. Gosling, J. T. Steinberg, D. J. McComas, C. W. Smith, N. F. Ness, Q. Hu, and L. F. Burlaga (2004), Extremely high speed solar wind: 29–30 October 2003, *J. Geophys. Res.*, *109*, A09102, doi:10.1029/2004JA010494.

Smith, C. W., J. L'Heureux, N. F. Ness, M. H. Acuna, L. F. Burlaga, and J. Scheifele (1999), The ACE Magnetic Fields Experiment, *Space Sci. Rev.*, *86*, 613, doi:10.1023/A:1005092216668.

Strangeway, R. J., C. T. Russell, C. W. Carlson, J. P. McFadden, R. E. Ergun, M. Temerin, D. M. Klumpar, W. K. Peterson, and T. E. Moore (2000), Cusp field-aligned currents and ion outflows, *J. Geophys. Res.*, *105*, 21,129–21,141, doi:10.1029/2000JA900032.

Swider, W. (1990), Precipitating and trapped ions and electrons observed at 840 km during the Great Magnetic Storm of February 1986, *J. Geophys. Res.*, *95*(A7), 10,417–10,425, doi:10.1029/JA095iA07p10417.

Thomsen, M., C. A. Cattell, B. Lavraud, J. E. Borovsky, and J. Dombeck (2004), Energized ions in the dayside magnetosphere during the SEC events of late October 2003, EOS Trans. AGU, SH42A-05, AGU Spring 2004.

Winningham, J. D., J. L. Burch, and R. A. Frahm (1984), Bands of ions and angular V's: A conjugate manifestation of ionospheric ion acceleration, *J. Geophys. Res.*, *89*, 1749–1754, doi:10.1029/JA089iA03p01749.

Wygant, J., F. Mozer, M. Temerin, J. Blake, N. Maynard, H. Singer, and M. Smiddy (1994), Large amplitude electric and magnetic field signatures in the inner magnetosphere during injection of 15 MeV electron drift echoes, *Geophys. Res. Lett.*, *21*, 1739–1742, doi:10.1029/94GL00375.

Yamauchi, M., Y. Ebihara, I. Dandouras, and H. Reme (2009), Dual source populations of substorm-associated ring current ions, *Ann. Geophys.*, *27*, 1431–1438, doi:10.5194/angeo-27-1431-2009.

Yao, Y., K. Seki, Y. Miyoshi, J. P. McFadden, E. J. Lund, and C. W. Carlson (2008), Statistical properties of the multiple ion band structures observed by the FAST satellite, *J. Geophys. Res.*, *113*, A07204, doi:10.1029/2008JA013178.